NASA TECHNIC
MEMORANDUM

N 7 3   3 0 7 9 5

NASA TM X-64768

SPACE SHUTTLE
  o RENDEZVOUS
  o RADIATION
  o REENTRY
ANALYSIS CODE

By Dave M. McGlathery
Aero-Astrodynamics Laboratory

May 16, 1973

NASA

George C. Marshall Space Flight Center
Marshall Space Flight Center, Alabama

1. REPORT NO. NASA TM X-64768	2. GOVERNMENT ACCESSION NO.	3. RECIPIENT'S CATALOG NO.
4. TITLE AND SUBTITLE Space Shuttle Rendezvous, Radiation and Reentry Analysis Code		5. REPORT DATE May 16, 1973
		6. PERFORMING ORGANIZATION CODE
7. AUTHOR(S) Dave M. McGlathery		8. PERFORMING ORGANIZATION REPORT #
9. PERFORMING ORGANIZATION NAME AND ADDRESS George C. Marshall Space Flight Center Marshall Space Flight Center, Alabama 35812		10. WORK UNIT, NO.
		11. CONTRACT OR GRANT NO.
		13. TYPE OF REPORT & PERIOD COVERED
12. SPONSORING AGENCY NAME AND ADDRESS National Aeronautics and Space Administration Washington, D.C. 20546		Technical Memorandum
		14. SPONSORING AGENCY CODE

15. SUPPLEMENTARY NOTES

Prepared by Aero-Astrodynamics Laboratory,
Science and Engineering

16. ABSTRACT

Documented in this report is the development of a preliminary Space Shuttle Mission Design and Analysis Tool emphasizing versatility, flexibility, and user interaction through the use of a relatively small computer (IBM-7044). The Space Shuttle Rendezvous, Radiation and Reentry Analysis Code is used to perform mission and space radiation environmental analyses for four typical Space Shuttle missions. Included also is a version of the proposed Apollo/Soyuz Rendezvous and Docking Test Mission. Tangential steering circle to circle low-thrust tug orbit raising and the effects of the trapped radiation environment on trajectory shaping due to solar electric power losses are also features of this mission analysis code.

The computational results include a parametric study on single impulse versus double impulse deorbiting for relatively low Space Shuttle orbits as well as some definitive data on the magnetically trapped protons and electrons encountered on a particular mission.

17. KEY WORDS Integrated trajectories Free and powered flight Retrograde deorbiting Mission abort deorbiting Atmospheric reentry angles Orbiter ground trace	Landing site acquisition Space radi- ation effects	18. DISTRIBUTION STATEMENT Unclassified-unlimited E. H. Geissler E. D. GEISSLER Director, Aero-Astrodynamics Laboratory

19. SECURITY CLASSIF. (of this report) Unclassified	20. SECURITY CLASSIF. (of this page) Unclassified	21. NO. OF PAGES 95	22. PRICE NTIS

TABLE OF CONTENTS

LIST OF ILLUSTRATIONS

LIST OF ILLUSTRATIONS (Continued)

LIST OF ILLUSTRATIONS (Concluded)

LIST OF TABLES

DEFINITION OF SYMBOLS

Symbol	Definition
a	semimajor axis
a_D	deorbit conic — semimajor axis
$a_{i,j}$	elements of transformation matrix from geocentric to nodal launch coordinates
$|\overline{A}|$	magnitude of areal velocity vector
A	total area of the orbital ellipse
$A_{i,j}$	elements of transformation matrix from geocentric reference axes to orbit plane axes
b	semiminor axis
β	launch azimuth
$\beta*$	instantaneous cross-range angle
$d_i \ (i=1\ldots N)$	directrix distances of the ellipse from corresponding foci
e	eccentricity of any general orbit
e_D	eccentricity of deorbit conic
E	general eccentric anomaly
E_D	deorbit conic eccentric anomaly measured clockwise from perigee
G	universal gravitational constant $= 6.6732$ by 10^{-11} meters^3/sec^2-Kg
m	mass of central body (Earth) $= 5.97319$ by 10^{24} Kg
μ	product $Gm = 3.98603$ by 10^{14} meters^3/sec^2

viii

DEFINITION OF SYMBOLS (Continued)

Symbol	Definition
γ	flight path angle — measured from vertical extension of radius vector $\overline{r}$
γ_i^* (i=1,2...N)	atmosphere reentry angles
G_o	Greenwich Meridian reference intersection
$HA(G_o)$	angle as a function of time between Greenwich G_o and vernal equinox Υ reference points
$\overline{H}$	geocentric perpendical to orbital plane
h	twice the constant magnitude of areal velocity or angular momentum constant
i	inclination of the orbit
J_2	earth zonal harmonic term = 1.0827 by 10^{-3}
λ	geocentric longitude measured east and west of Greenwich
λ_I	geocentric insertion longitude
Λ	energy parameter — twice the ratio of kinetic to potential energy
Λ_a	energy parameter at apogee
Λ_{a_c}	energy parameter at apogee — circular orbit = 1
λ_L	geocentric longitude of launch site
Λ_a^*	new energy parameter value associated with incremental change in spacecraft velocity at apogee
Λ_p	energy parameter at perigee

DEFINITION OF SYMBOLS (Continued)

Symbol	Definition
Λ_{p_c}	energy parameter at perigee — circular orbit = 1
Λ_{p*}	new energy parameter value associated with incremental change in spacecraft velocity at perigee
Λ_o	energy parameter at some specific distance V_o with some specific spacecraft velocity V_o
$\overline{L}$	geocentric launch site vector
M	general mean anomaly
M_D	deorbit conic mean anomaly — measured clockwise from perigee
$\overline{N}$	geocentric perpendicular to plane containing $\overline{L}$ and $\overline{H}$
n	mean motion (Keplerian)
Δn	perturbed mean motion due to oblate earth
$n*$	corrected mean motion for oblate earth
ω	argument of perigee
$\omega*$	nodal anomaly — angle that radius vector sweeps measured the nodal vector $\overline{r}_{\Omega*}$
$\dot{\omega}$	rate of perigee procession or regression due to an oblate earth
$\overline{\omega}_e$	rotation rate of the earth = .004178074216 deg/sec
Ω	right ascension of ascending node measured from the vernal equinox reference point
$\Omega*$	longitude of the node measured from the Greenwich meridian reference point
$\Omega*(t)$	changing longitude of the node angle as a function of time

DEFINITION OF SYMBOLS (Continued)

Symbol	Definition
Ω^*_a	longitude of the ascending node measured from Greenwich
Ω^*_d	longitude of the descending node measured from Greenwich
$\dot{\Omega}$	rate of nodal regression due to an oblate earth
P_D	period of deorbit conic
$\overline{P}$	projection of $\overline{L}$ on the orbital plane
p	semilatus rectum of ellipse
π	number of radian in semi-circle
Φ	geocentric latitude
Φ_L	geocentric launch site latitude
Φ_I	geocentric insertion latitude
Θ	true anomaly
Θ^*	instantaneous down range angle
r	magnitude of focal radius vector
$\overline{r}$	focal radius vector
r_a	radius of apogee
r_p	radius of perigee
r_{a_t}	radius of apogee for transfer orbit
r_{p_t}	radius of perigee for transfer orbit

DEFINITION OF SYMBOLS (Continued)

Symbol	Definition
$r_{a_{fc}}$	radius of apogee for final circular orbit
$r_{p_{fc}}$	radius of perigee for final circular orbit
r_{p_i} (i=1,2...N)	radius of perigee for deorbit conics
r_{a_c}	radius of apogee for circular orbit
r_{p_c}	radius of perigee for circular orbit
$\overline{R}_E$	geocentric radius vector
R_E	magnitude of earth's geocentric radius = 6378.160 Km
$\overline{R}_D$	geocentric radius from center of earth to reentry point on deorbit conic
$\overline{r}_c$	focal radius vector for circular orbit
r_o	any specified distance along orbital path
r_b	focal radius to minor axis point
t	time of flight along orbital path
τ	time of perigee passage
t_o	starting time for orbit insertion
t_D	time of flight along deorbit conic
T	Keplerian period of an orbit
T^*	perturbed period due to an oblate earth

DEFINITION OF SYMBOLS (Continued)

Symbol	Definition
T_D	time of flight along deorbit conic from retrofire to reentry target point
Υ	first point of aries — vernal equinox
V	linear speed of an orbiting body
$\overline{V}$	velocity vector
V_A	linear scalar speed at apogee
V_p	linear scalar speed at perigee
V_c	circular orbit scalar speed
ΔV	velocity change increment — increase or decrease requiring a specific amount of propellant
X, Y, and Z	general reference coordinates
X_G, Y_G, or Z_G	geocentric reference coordinate axes
$\overline{i}$, $\overline{j}$, and $\overline{k}$	unit vectors along geocentric reference coordinate axes
X_o, Y_o, and Z_o	orbital plane coordinate axes
$\overline{i}_o$, $\overline{j}_o$, and $\overline{K}_o$	unit vectors along orbital plane coordinate axes
X''', Y''', and Z'''	first intermediate coordinate axes after a rotation about an axes
X'', Y'', and Z''	second intermediate coordinate axes after a rotation about an axes
X', Y', and Z'	final coordinate axes after all rotations are complete

DEFINITION OF SYMBOLS (Continued)

Symbol	Definition
(X, Y, Z)	instantaneous position of spacecraft in geocentric Cartesian coordinates
(r, Φ, λ)	instantaneous positions of spacecraft in spherical (geocentric) coordinates
(X_o, Y_o, Z_o)	instantaneous position of spacrcraft in orbital plane coordinates
(Y_L, Φ_L, λ_L)	launch and landing site geocentric spherical coordinates
$(\dot{X}_G, \dot{Y}_G, \dot{Z}_G)$	components of the velocity vector in geocentric coordinates
$(\ ^\cdot) = \dfrac{d}{dt}(\ )$	time derivative
$d(\ )$	differential
$(\ ) \times (\ )$	vector cross product
$(\ ) \cdot (\ )$	vector scaler product
$\lvert(\ )\rvert$	vector magnitude
(B, L)	two-dimensional magnetic field coordinate system where B denotes the magnetic field strength (gauss) and L denotes a distance (earth radii) that describes a magnetic shell
$F(B, L)$	particle flux intensity at a point in space
e	exponential
E_1	lower energy range of interest — MeV (million electrons volts)
E	specific or upper energy range of interest
$E_o(B, L)$	exponential shaping parameter of the particle differential and integral spectrums

DEFINITION OF SYMBOLS (Concluded)

Symbol	Definition
$J(>E, B, L)$	omnidirectional integral flux spectrum at a point in space
$J'(E, B, L)$	omnidirectional differential energy spectrum at a point in space
$\bar{J}(>E)$	time averaged integral energy spectrum
$\bar{J}(>E_1)$	time averaged integral spectrum for all particles greater than lower cut-off energy
$\bar{J}(E)$	time averaged differential energy spectrum
t_o	beginning time for time averaged calculations
t_n	ending time for time averaged calculations

SPACE SHUTTLE RENDEZVOUS, RADIATION AND REENTRY ANALYSIS CODE

SECTION I. INTRODUCTION

The austerity of the total space budget and the need to continue meaningful space-oriented scientific research demanded the development of a reusable Space Shuttle System. Comprehensive and detailed mission analysis for such a system is required to provide the kind of vehicle design and mission integration data needed during Phase A and B studies and beyond, to ensure the development of a Space Shuttle System that performs as intended.

The purpose of this effort was to develop a comprehensive, unified and versatile mission design and analysis tool which could be economically used to provide the kind of data mentioned above for preliminary investigations of the Space Shuttle System. This document may also serve as a ready reference for near earth orbital analysis and various parametric studies.

The underlying philosophy of approach in developing this computer program was to produce a self-contained, multipurpose, multioutput package, placing emphasis on accessibility and usability with a minimum of input preparations, while constraining accuracy within acceptable tolerances, thereby economizing with regard to computer run time.

The Space Shuttle Rendezvous, Radiation and Reentry Analysis Code has been developed, checked out and used to provide some preliminary data for proposed earth resources Sortie Lab experiments. This document is not intended as a user's manual but rather to describe the mathematical model used and to give insight on the applicability of this Mission Analysis Code to a certain class of problems involving the Space Shuttle System. A complete program listing is available upon request.

The Space Shuttle reentry analysis includes giving instantaneous reentry and landing site acquisition constraint parameters, all as a function of a specific range of atmospheric reentry angles and the reentry target altitude. Thus, suitable reentry conditions are achieved for the Orbiter at the beginning of reentry proper; i.e., at the start of its plunge through the dense atmosphere.

Section II gives a complete description of the Space Shuttle Mission Analysis code, including the mathematical modeling of the systems geometry and equations. Also, specific input-output options are detailed.

Section III presents data generated using the Space Shuttle Mission Analysis Code to perform rendezvous radiation and reentry analysis, simulating five examples of Space Shuttle missions. It is divided into three major parts. Part A gives the results of parametric two-dimensional study on single impulse versus double impulse deorbiting for the Space Shuttle with constraints in the range of allowable atmospheric reentry angles and velocities at the reentry target altitude due to vehicle heating considerations. Also, the relative orbital manuevering system ΔV requirement is parameterized for deorbiting from varying altitudes and achieving reentry angles over the indicated range. Part B illustrates the results of performing three-dimensional mission analysis for five typical space Shuttle missions including a version of the proposed Apollo/ Soyuz Rendezvous and Docking Test Mission. Part C shows the results of the space radiation analyses of magnetically trapped protons and electrons encountered during specific missions simulated in Part B.

SECTION II. PROGRAM DESCRIPTION (SYSTEMS GEOMETRY AND EQUATIONS)

Methods of orbital analysis and trajectory generation are many and varied. For preliminary analysis it is usually sufficient to perform basically a two-body Keplerian analysis with minimum effects, due to perturbing forces of some prescribed nature. There is a direct transformation between the six-dimensional space of Cartesian coordinates X, Y, Z, $\dot{X}$, $\dot{Y}$, $\dot{Z}$ and the six classical orbital elements a, e, τ, Ω, ω, and i.

A basic approach to trajectory generation, then, is to define an initial set of orbital elements along with any pertinent or secular time rates of changes of the elements, thus iterating between the two frames of reference performing the desired mapping of position and velocity at any instant of time.

This section illustrates the coordinate system geometry and defines the equations used in constructing the mathematical models employed by the Space Shuttle Rendezvous, Radiation and Reentry Analysis Code to perform orbital analysis and trajectory generation for the Space Shuttle System.

2

In some instances only general geometric and functional relationships are presented because the detailing of specific manipulations is only pertinent to the actual programming effort.

A. Basic Two-Body Geometry and Dynamics

1. **Orbital Plane Geometry.** By definition of the properties of an ellipse, the following basic relationships are immediately derived from Figure 1, assuming the variables a, e and Θ are available inputs:

$$r = a(1-e^2)/1+e \cos \Theta \qquad (1)$$

$$p = a(1-e^2) \qquad (2)$$

$$b = a(1-e^2)^{1/2} \qquad (3)$$

where, by classic definition

e = eccentricity

a = semimajor axis

b = semiminor axis

p = semilatus rectum

Θ = true anomaly

r = radius vector from focus

From equation (1), with $\Theta = 0°$ and $180°$ respectively, we obtain

$$r_p = p/(1+e) = a(1-e) \qquad (4)$$

$$r_a = p/(1-e) = a(1+e) \qquad (5)$$

which gives functional values for the radius of perigee and the radius of apogee, respectively.

3
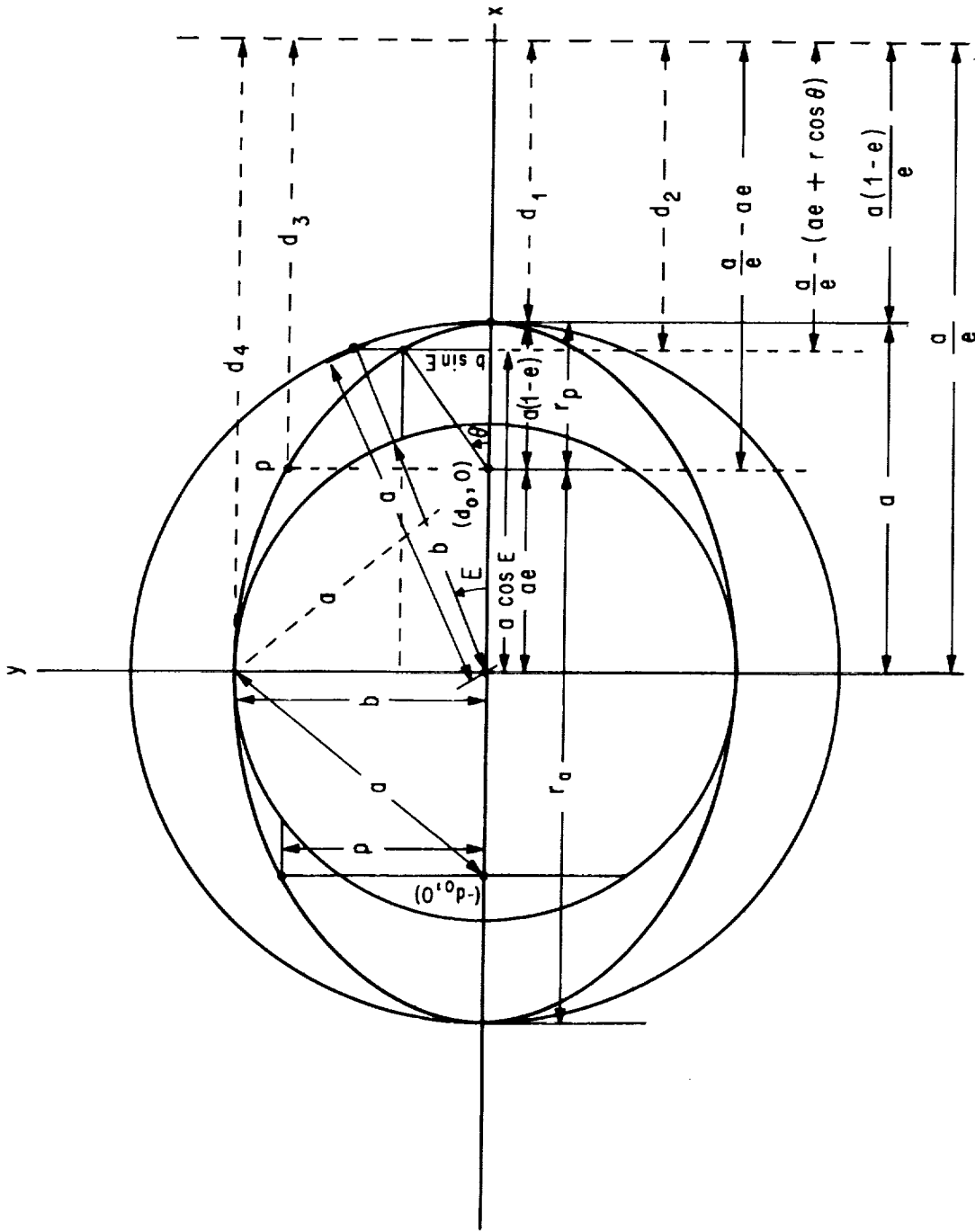
Figure 1. Orbital plane geometry.

4

Again from Figure 1 expressing the rectangular coordinates (X_o, Y_o) of the orbital plane as a function of the eccentric anomaly E and the true anomaly Θ, gives rise to the following relationships between E and Θ:

$$\cos E = \frac{e + \cos \Theta}{1 + e \cos \Theta} = \frac{a - r}{ae} \tag{6}$$

and

$$\sin E = \frac{\left(1-e^2\right)^{1/2} \sin \Theta}{1 + e \cos \Theta} \tag{7}$$

The focal radius equation thus becomes

$$r = a(1-e \cos E) \tag{8}$$

The total area A of the ellipse integrated over E gives rise to an angular parameter mean anomaly M

$$M = E - e \sin E \tag{9}$$

which is defined as a central angle compared to a circle having the same total area as the ellipse.

2. <u>Central Force Field Dynamics.</u> The areal velocity or angular momentum vectors with the magnitude expressed in polarform reduces to

$$|\overline{A}| = \tfrac{1}{2} |\overline{r} \times \overline{v}| = \tfrac{1}{2} r^2 \dot{\Theta} = \frac{h}{2} = \text{constant} \tag{10}$$

This property permits the differential equation of motion to be easily derived, thus establishing the following parametric relationships

$$p = \frac{h^2}{\mu} \tag{11}$$

from which

$$h = [a(1-e^2)\mu]^{1/2} \qquad (12)$$

where $\mu = Gm$, G being the universal gravitational constant and m the mass of the central body.

Comparing the properties of equation (10) to the total integrated area of an ellipse and using previously defined quantities, we obtain the general time of flight equation

$$t = \sqrt{\frac{a^3}{\mu}} \ (E - e \sin E) \qquad (13)$$

Thus, the total time for one revolution of an orbit is

$$T = 2\pi \sqrt{\frac{a^3}{\mu}} \qquad (14)$$

The mean motion n defines the average angular rate of a body in orbit and is given from equation (14) to be

$$n = \frac{2\pi}{T} = \sqrt{\frac{\mu}{a^3}} \qquad (15)$$

where the units of n are radius per unit time.

The mean anomaly M can now be defined also as a function of mean motion

$$M = n(t - \tau) \qquad (16)$$

where τ is the time of perigee passage.

6

Comparison of equation (9) and (16) yields

$$M = n(t - \tau) = E - e \sin E \tag{17}$$

Thus, M is readily obtained when $(t - \tau)$ is given and a good approximation of E can be found when M is known from the following series expansion

$$E = M + e \sin M + \frac{e^2 \sin 2M}{2} + \ldots \tag{18}$$

A general expression for the instantaneous linear speed of the orbiting body is derived from equation (10) to be

$$V = \frac{h}{r \sin \gamma} \tag{19}$$

where γ is the angle between $\overline{r}$ and $\overline{v}$ and is called the flight path angle.

3. Two Body Energy Relationships. A very useful computational energy parameter will be introduced and defined as

$$\Lambda = \frac{r v^2}{\mu} \tag{20}$$

where Λ is twice the ratio of kinetic to potential energy of the orbiting body. The semimajor axis may be defined now as

$$a = \frac{r}{2 - \Lambda} \tag{21}$$

and the eccentricity becomes

$$e = \sqrt{1 - \Lambda(2 - \Lambda)\sin^2\gamma} \qquad (22)$$

also the semilatus rectum can be written as

$$p = \frac{h^2}{\mu} = \frac{r^2 v^2 \sin^2\gamma}{\mu} = r\Lambda \sin^2\gamma \qquad . \qquad (23)$$

Thus, it is seen that the orbit-shaping parameters may be determined as a function of Λ and γ. Using the above relationships, still another focal radius equation may be written:

$$r = \frac{r_o \Lambda_o \sin^2\gamma_o}{1 + \sqrt{1 - \Lambda_o(2 - \Lambda_o)\sin^2\gamma_o}\cos\Theta_o} \qquad . \qquad (24)$$

Equation (24) is a very practical tool for computing the range of ballistic trajectories by treating them as fictitious orbits about the earth.

Applying certain initial conditions along the major axis of the orbit as shown in Figure 2, some useful computational relationships become evident. Perigee injection equation (24) becomes

$$\frac{r_a}{r_p} = \frac{\Lambda_p}{1 - \sqrt{1 - \Lambda_p(2 - \Lambda_p)}} \qquad . \qquad (25)$$

Solving equation (25) for Λ_p, we obtain as one solution

$$\Lambda_p = \frac{2 r_a(r_p - r_a)}{r_p^2 - r_a^2} \qquad (26)$$

which defines Λ_p as a function of desired r_a. For the circular orbit

8
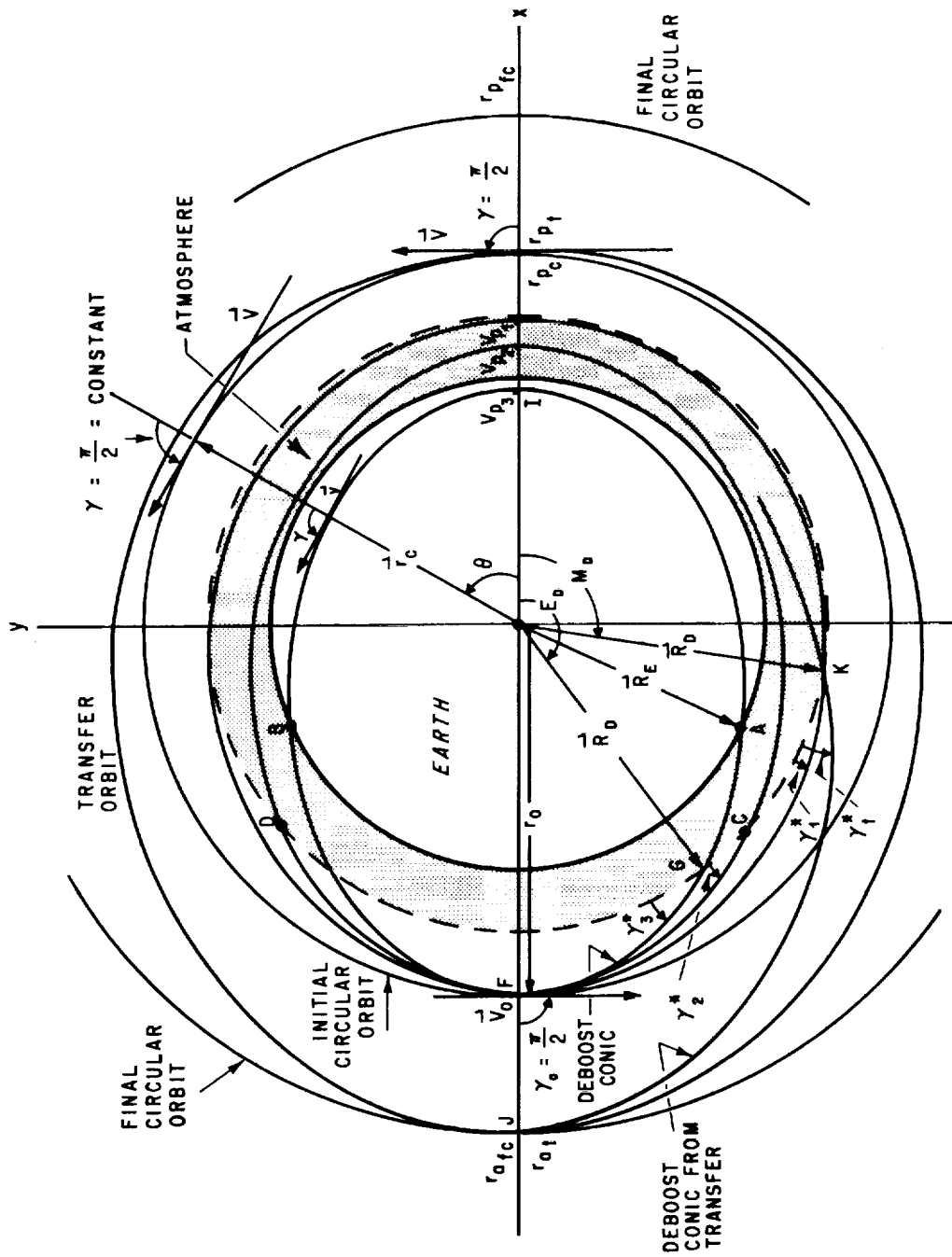
Figure 2. Coplanar rendezvous and reentry geometry.

9

$$\Lambda_{p_c} = \frac{r_a}{r_p} = 1 \quad .$$
(27)

Proceeding in a similar manner for apogee injection we have

$$\Lambda_a = \frac{2 r_p (r_p - r_a)}{r_p^2 - r_a^2}$$
(28)

defining also Λ_a as a function of the desired r_p. Again for the circular orbit case

$$\Lambda_{a_c} = \frac{r_p}{r_a} = 1$$
(29)

the ratio of Λ_a to Λ_p reveals a useful relationship for tying down an orbit. From equation (26) and (28) we obtain

$$\Lambda_p = \frac{r_a}{r_p} \Lambda_a$$
(30)

and

$$\Lambda_a = \frac{r_p}{r_a} \Lambda_p \quad .$$
(31)

This gives the capability to determine the energy parameter value at the opposite end of the major axis of a specific orbit when the value for either end is known. Also the energy parameter values Λ_p and Λ_a are directly related to the satellite velocities at each point, i.e., at perigee V_p and at apogee V_a.

10

4. <u>Time of Flight Computation Along Reentry Path.</u> The time of flight
parameter from deorbit retro fire to some specified reentry target point as
shown in Figure 2 will vary depending on the desired atmospheric reentry
angle γ^* and the altitude of the deorbit manuever. The specific problem, then,
is to define the time it takes to go from point F to point G, or from point J to
point K of Figure 2 after retro fire.

Using the equations of Section I, we can express the time it takes to go
from point H to point G of the deorbit conic shown in Figure 2 as

$$t_D = \frac{P_D \, M_D}{2\pi} \tag{32}$$

where P_D and M_D is the period and mean anomaly of the deorbit conic respec-
tively. Therefore, the time of flight from point F to point G may be expressed
as

$$T_D = \frac{P_D}{2} - \frac{P_D \, M_D}{2\pi} \tag{33}$$

which reduces to

$$T_D = \sqrt{\frac{a_D^{\,3}}{\mu}} \; (\pi - M_D) \tag{34}$$

where M_D is computed from equations (6) and (17)

B. Orientation of the Orbital Plane
and Trajectory Generation

The orientation parameters are designated Ω, longitude of the ascending
node; ω, the angle or argument of perigee and i, the inclination of the orbit.

Figure 3 shows the particular frame of reference used in the Space Shuttle Mission Analysis Code to describe the relative position of the spacecraft.

The reference longitude is the Greenwich meridian point G_o or the Greenwich hour angle at the time of launch or insertion. The time-varying ascending node angle $\Omega*$ is indicated as a function of rotational rate of the earth, $\overline{\omega}_e$ and the nodal regression rate $\dot{\Omega}$ of the particular orbit.

$$\Omega*(t) = \Omega*_o + (\overline{\omega}_e + \dot{\Omega}) t \qquad (35)$$

where $\Omega*_o$ is the instantaneous value at $t_o = 0$; i.e., at launch or insertion and t is the elapsed time since t_o.

The position and velocity components of the system as a function of time are thus described by performing the indicated axes rotations of Figure 3 which is a transformation from orbital coordinates to geocentric Cartesian coordinates.

Iterative or successive use of these transformation equations with the time-varying orbital elements serve to generate desired Space Shuttle trajectories.

The three indicated rotations will be performed in the following order: (1) a positive rotation through angle $\Omega*$ about the z-axis (2) a positive rotation through angle i about the new x-axis, i.e., X''', and (3) a positive rotation through angle ω about the new z-axis, i.e., Z''.

The matrix operation that completes the transformation from geocentric to orbital coordinates is then

$$
\begin{pmatrix} X_o \\ Y_o \\ Z_o \end{pmatrix} =
\begin{pmatrix} \cos\omega & \sin\omega & 0 \\ -\sin\omega & \cos\omega & 0 \\ 0 & 0 & 1 \end{pmatrix}
\begin{pmatrix} 1 & 0 & 0 \\ 0 & \cos i & \sin i \\ 0 & -\sin i & \cos i \end{pmatrix}
\begin{pmatrix} \cos\Omega* & \sin\Omega* & 0 \\ -\sin\Omega* & \cos\Omega* & 0 \\ 0 & 0 & 1 \end{pmatrix}
\begin{pmatrix} X_G \\ Y_G \\ Z_G \end{pmatrix} \qquad (36)
$$

12

Figure 3. Geocentric reference coordinate system.

13

Performing the above indicated matrix operation yields

$$\begin{pmatrix} X_o \\ Y_o \\ Z_o \end{pmatrix} = \begin{pmatrix} A_{11} & A_{12} & A_{13} \\ A_{21} & A_{22} & A_{23} \\ A_{31} & A_{32} & A_{33} \end{pmatrix} \begin{pmatrix} X_G \\ Y_G \\ Z_G \end{pmatrix} \qquad (37)$$

where the elements of matrix equation (37) are defined to be:

$$A_{11} = \cos \omega \, \cos \Omega^* - \sin \omega \, \cos i \, \sin \Omega^*$$

$$A_{12} = \cos \omega \, \sin \Omega^* + \sin \omega \, \cos i \, \cos \Omega^*$$

$$A_{13} = \sin \omega \, \sin i$$

$$A_{21} = - \sin \omega \, \cos \Omega^* - \cos \omega \, \cos i \, \sin \Omega^*$$

$$A_{22} = - \sin \omega \, \sin \Omega^* + \cos \omega \, \cos i \, \cos \Omega^*$$

$$A_{23} = \cos \omega \, \sin i$$

$$A_{31} = \sin i \, \sin \Omega^*$$

$$A_{32} = \sin i \, \cos \Omega^*$$

$$A_{33} = \cos i$$

To solve for geocentric coordinates we need the inverse form of our rotation matrix which for orthogonal coordinate systems is just the transpose of the rotation matrix.

Substituting also the derived relationships between the orbital plane coordinates (X_o, Y_o) and the eccentric anomaly E from Figure 1, we obtain for geocentric rectangular coordinates:

14

$$\begin{pmatrix} X_G \\ Y_G \\ Z_G \end{pmatrix} = \begin{pmatrix} A_{11} & A_{21} & A_{31} \\ A_{12} & A_{22} & A_{32} \\ A_{13} & A_{23} & A_{33} \end{pmatrix} \begin{pmatrix} a(\cos E - e) \\ a(1-e^2)^{1/2} \sin E \\ 0 \end{pmatrix} \tag{38}$$

Differentiating each of the three component equations of matrix equation (38) with respect to time and solving for $\dot{E}$ by differentiating equation (13) with respect to time, we obtain the velocity components in geocentric coordinates as a function of eccentric anomaly E.

$$\begin{pmatrix} \dot{X}_G \\ \dot{Y}_G \\ \dot{Z}_G \end{pmatrix} = \begin{pmatrix} A_{11} & A_{21} & A_{31} \\ A_{12} & A_{22} & A_{32} \\ A_{13} & A_{23} & A_{33} \end{pmatrix} \begin{pmatrix} -a \sin E \ \dfrac{n}{1-e \cos E} \\ a(1-e^2)^{1/2} \cos E \ \dfrac{n}{1-e \cos E} \\ 0 \end{pmatrix} \tag{39}$$

Position and velocity components as a function of the true anomaly Θ also fall out directly in a similar manner, yielding

$$\begin{pmatrix} X_G \\ Y_G \\ Z_G \end{pmatrix} = \begin{pmatrix} A_{11} & A_{21} & A_{31} \\ A_{12} & A_{22} & A_{32} \\ A_{13} & A_{23} & A_{33} \end{pmatrix} \begin{pmatrix} r \cos \Theta \\ r \sin \Theta \\ 0 \end{pmatrix} \tag{40}$$

and for the velocity components

$$\begin{pmatrix} \dot{X}_G \\ \dot{Y}_G \\ \dot{Z}_G \end{pmatrix} = \begin{pmatrix} A_{11} & A_{21} & A_{31} \\ A_{12} & A_{22} & A_{32} \\ A_{13} & A_{23} & A_{33} \end{pmatrix} \begin{pmatrix} \dfrac{-na \sin \Theta}{(1-e^2)^{1/2}} \\ \dfrac{na(\cos \Theta + e)}{(1-e^2)^{1/2}} \\ 0 \end{pmatrix} \tag{41}$$

15

Since we have computed the position of the orbiting body in rectangular coordinates, positions in spherical coordinates (r, Φ, λ) are obtained from the transformation shown in Figure 4:

$$r = \sqrt{X^2 + Y^2 + Z^2} \tag{42}$$

$$\sin \Phi = \frac{Z}{r} \tag{43}$$

$$\tan \lambda = \frac{Y}{X} \tag{44}$$

with the inverse relation being

$$X = r \cos \Phi \cos \lambda \tag{45}$$

$$Y = r \cos \Phi \sin \lambda \tag{46}$$

$$Z = r \sin \Phi \tag{47}$$

C. Orbit Determination From Initial Launch Site and Orbit Insertion Conditions

The methods of orbital analysis presented in Section II, Part B, assumed an initial set of orbital elements a_o, e_o, τ_o, ω_o, Ω_o^*, and i_o. It may be, however, that the only initial conditions information available is (1) launch site geocentric spherical coordinates (r_L, Φ_L, λ_L), (2) launch azimuth (3) the desired (r, v, γ) for orbit insertion and (4) the orbit insertion geocentric spherical coordinates (r_I, Φ_I, λ_I). The problem is then to obtain an initial set of dimensional and orientation orbital elements from this set of given information. Certain indicated constraints placed on some of the insertion parameters serve the purpose of simplification of method; however, the removal of these constraints does not add unduly to the complexity of the problem's solution.

16

Figure 4. Spherical – rectangular coordinate transformations.

Once the initial set of orbital elements is obtained, the methods of orbital analysis and trajectory generation presented in Section II, Part B, are then initiated.

Referring to Figure 5, the spherical coordinates (r_L, Φ_L, λ_L) are the launch site coordinates. The unit vectors $(\bar{i}_o, \bar{j}_o, \bar{k}_o)$ define the orbital axes and the unit vectors $(\bar{i}_G, \bar{j}_G, \bar{k}_G)$ define the geocentric coordinate axes. The spacecraft is launched from the designated site with the velocity vector lying along the launch azimuth β with flight path angle γ. All initial conditions are referred to the orbit insertion point; i.e., at perigee. The flight path angle γ will thus be $\frac{\pi}{2}$ and the actual orbit insertion point will be a down-range angle Θ^* from the launch site. It is further established by definition that $\bar{i}_o$ will lie along $\bar{r}_L$; $\bar{j}_o$ will lie along the launch azimuth and $\bar{k}_o$ will lie along the launch site meridian pointing north. Planar flight is assumed and when the actual flight is not planar, adjustments are necessary in the initial defining orbital elements. The transformation matrix from geocentric to nodal launch coordinate is obtained from the indicated rotation of Figure 5:

(1)   a positive rotation about $\bar{k}_G$ through angle λ

(2)   a negative rotation about the new $\bar{j}$ axis; i.e., $\bar{j}'$ through angle $-\Phi_L$, and

(3)   a positive rotation about $\bar{i}''$ through the angle $(90-\beta)$ which joins the two coordinate systems to coincide.

The resulting matrix operation will then be

$$
\begin{pmatrix} X_o \\ Y_o \\ Z_o \end{pmatrix} = \begin{pmatrix} 1 & 0 & 0 \\ 0 & \sin\beta & \cos\beta \\ 0 & -\cos\beta & \sin\beta \end{pmatrix} \begin{pmatrix} \cos\Phi_L & 0 & \sin\Phi_L \\ 0 & 1 & 0 \\ -\sin\Phi_L & 0 & \cos\Phi_L \end{pmatrix} \begin{pmatrix} \cos\lambda_L & \sin\lambda_L & 0 \\ -\sin\lambda_L & \cos\lambda_L & 0 \\ 0 & 0 & 1 \end{pmatrix} \begin{pmatrix} X_G \\ Y_G \\ Z_G \end{pmatrix}
$$

(48)

which yields
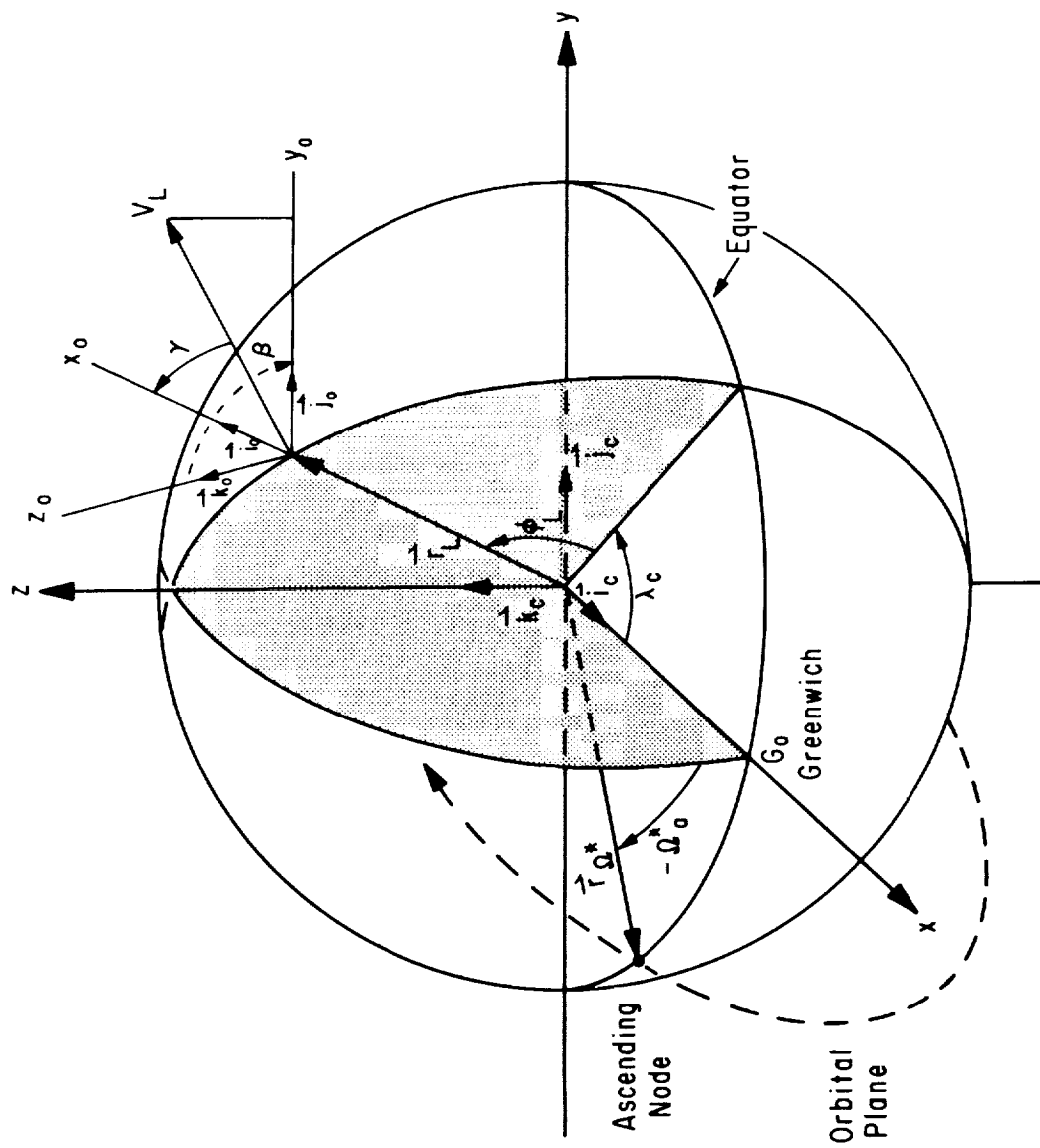
Figure 5. Orbit determination geometry from initial launch conditions.

19

$$
\begin{pmatrix} X_O \\ Y_O \\ Z_O \end{pmatrix} = \begin{pmatrix} a_{11} & a_{12} & a_{13} \\ a_{21} & a_{22} & a_{23} \\ a_{31} & a_{32} & a_{33} \end{pmatrix} \begin{pmatrix} X_G \\ Y_G \\ Z_G \end{pmatrix}
\tag{49}
$$

where

$$a_{11} = \cos \Phi_L \cos \lambda_L$$

$$a_{12} = \cos \Phi_L \sin \lambda_L$$

$$a_{13} = \sin \Phi_L$$

$$a_{21} = -\sin \beta \sin \lambda_L - \cos \beta \sin \Phi_L \cos \lambda_L$$

$$a_{22} = \sin \beta \cos \lambda_L - \cos \beta \sin \Phi_L \sin \lambda_L$$

$$a_{23} = \cos \beta \cos \Phi_L$$

$$a_{31} = \cos \beta \sin \lambda_L - \sin \beta \sin \Phi_L \cos \lambda_L$$

$$a_{32} = -\cos \beta \cos \lambda_L - \sin \beta \sin \Phi_L \sin \lambda_L$$

$$a_{33} = \sin \beta \cos \Phi_L$$

Element a_{33} of matrix equation (49) gives the direction cosine for the angle between k_G and k', thus defining the inclination of the orbit:

$$\overline{k}_G \cdot \overline{k}' = \cos i = \sin \beta \cos \Phi_L \quad . \tag{50}$$

From Figure 5 the unit vector along the line of nodes in the equatorial plane may be defined as

$$\overline{r}_{\Omega *} = \cos \Omega * \, \overline{i} + \sin \Omega * \, \overline{j} \quad . \tag{51}$$

This vector transforms into orbital axes by the use of rotation matrix equation (49) and we obtain

$$\bar{k}_o = a_{31} \cos \Omega^* + a_{32} \sin \Omega^*$$

which leads to the relationship

$$\text{Tan } \Omega^* = \frac{\tan \lambda_L - \tan \beta \sin \Phi_L}{1 + \tan \beta \tan \lambda_L \sin \Phi_L} \qquad . \qquad (52)$$

If the first nodal crossing is a descending node, the ascending node is simply

$$\Omega^*_a = \Omega^*_D \pm 180° \qquad (53)$$

depending on whether Ω^*_D is east or west of Greenwich.

For a due east launch $\beta = 90°$ and the nodal longitude becomes from equation (52):

$$\text{Tan } \Omega^* = \text{Tan } (90° + \lambda_L) \qquad (54)$$

which reduces to

$$\Omega^* = 90° + \lambda_L \qquad (55)$$

giving a simple relationship for descending nodal crossing as a function of launch site longtitude.

From Figure 5 an angle ω^* is defined. The relationship between ω^* and ω is

$$\omega = \omega^* - \Theta \qquad (56)$$

at perigee, Θ is equal to zero and we have

21

$$\omega \ = \ \omega^*$$

and

$$\overline{i}_0 \cdot \overline{r}_{\Omega^*} \ = \cos \omega^* \qquad .$$

Using matrix equation (29) we can define an initial angle ω

$$\cos \omega \ = \ \cos \Phi_I \left(\cos \Omega_a^* \cos \lambda_I \ + \ \sin \Omega_a^* \sin \lambda_I \right) \tag{57}$$

where λ_I is the insertion point longitude. Using previously defined relationships to compute shaping elements a, e and τ we are thus able to compute all necessary initial defining elements which leads to a starting state vector for the Space Shuttle Mission Analysis at a zero reference time. Defining the variation of these elements with time enables us to compute a ground trace of the satellite's position at any time beyond t_o as depicted in Section II, Part B.

D. Formulation and Application of Certain Perturbing Effects on Keplerian Two-Body Motion

Since the Space Shuttle Mission Analysis Code is concerned with preliminary orbital analysis, only limited use will be made of general perturbation theory and application affecting the motion of a Keplerian orbit.

However, we may define with these analyses such effects as those due to (1) the oblateness of the Earth (2) a low thrust force vector (3) atmospheric drag and (4) a potential produced by the presence of other bodies of significant masses. The problem thus becomes to define the time rates of change of the six orbital elements as a system of linear differential equation and the various forms of the equations depending on the nature and origin of the force.

We may write the general differential equation of motion for a perturbed Keplerian orbit as

$$\ddot{\overline{r}} + \frac{\mu \overline{r}}{r^3} \ = \ \nabla R \tag{58}$$

where R is the particular disturbing function and ∇ is the operator,

$$\nabla = \frac{\partial}{\partial x}\overline{i} + \frac{\partial}{\partial y}\overline{j} + \frac{\partial}{\partial z}\overline{k}.$$

If we designate α_i as being any dimensional element, a, e, M and β_i as being any orientation element, Ω, ω, i, and use the fact that $\overline{r} = f(t, \alpha_i, \beta_i)$, we may write using the method of variation of arbitrary constants,

$$\sum_i \frac{\partial \overline{r}}{\partial \alpha_i}\dot{\alpha}_i + \sum_i \frac{\partial \overline{r}}{\partial \beta_i}\dot{\beta}_i = 0 \qquad (59)$$

and $\qquad\qquad\qquad\qquad\qquad\qquad\qquad i = 1, 2, 3$

$$\sum_i \frac{\partial \dot{\overline{r}}}{\partial \alpha_i}\dot{\alpha}_i + \sum_i \frac{\partial \dot{\overline{r}}}{\partial \beta_i}\dot{\beta}_i = \nabla R \qquad (60)$$

The simultaneous solution of equations (59) and (60) produces the transformation between the six-dimensional Cartesian coordinate space and the defining orbital elements α's and β's as a function of time.

$$\sum_{i=1}^{3} \left\{ [\alpha_r, \alpha_i]\dot{\alpha}_i + [\alpha_r, \beta_i]\dot{\beta}_i \right\} = \frac{\partial R}{\partial \alpha_r} \qquad (61)$$

and $\qquad\qquad\qquad\qquad\qquad\qquad r = 1, 2, 3$

$$\sum_{i=1}^{3} \left\{ [\beta_r, \alpha_i]\dot{\alpha}_i + [\beta_r, \beta_i]\dot{\beta}_i \right\} = \frac{\partial R}{\partial \beta_r} \qquad (62)$$

Where any expression of the form $[\alpha, \beta]$ is defined as a Lagrangian bracket and is of the Jacobian form

$$[\alpha, \beta] = \sum_{xyz} \frac{\partial(X, \dot{X})}{\partial(\alpha, \beta)} \quad .$$

Using the explicit relationships of equations (36) through (41) in Section II, Part B, to obtain the differential coefficients of the direction — cosines, we resolve all the indicated Lagrangian brackets of equations (61) and (62) in explicit forms.

Making these substitutions we arrive at the six linear differential equations depicting the time rates of change of the defining orbital elements as a function of the particular nature of the disturbing function R.

$$\dot{a} = \frac{2}{na} \frac{\partial R}{\partial M} \tag{63}$$

$$\dot{e} = \frac{1}{na^2e} \left\{ (1-e^2) \frac{\partial R}{\partial M} - (1-e^2)^{1/2} \right\} \frac{\partial R}{\partial \omega} \tag{64}$$

$$\dot{M} = n - \left(\frac{1-e^2}{na^2e} \right) \frac{\partial R}{\partial e} - \frac{2}{na} \left(\frac{\partial R}{\partial a} \right)_M \tag{65}$$

$$\dot{\Omega} = \frac{1}{na^2 (1-e^2)^{1/2} \sin i} \frac{\partial R}{\partial i} \tag{66}$$

$$\dot{\omega} = \left(\frac{-\cos i}{na^2 \sin i (1-e^2)^{1/2}} \right) \frac{\partial R}{\partial i} + \left(\frac{(1-e^2)^{1/2}}{na^2e} \right) \frac{\partial R}{\partial e} \tag{67}$$

$$\frac{di}{dt} = \left(\frac{\cos i}{na^2 \sin i (1-e^2)^{1/2}} \right) \frac{\partial R}{\partial \omega} - \left(\frac{1}{na^2 \sin i (1-e^2)^{1/2}} \right) \frac{\partial R}{\partial \Omega} \tag{68}$$

To complete the analysis as it pertains to a specific problem, we need only to define R in an explicit form and take the indicated partial derivatives.

Now, having an initial set of orbital elements a_o, e_o, M_o, Ω_o, ω_o, i and knowing the time rates of change of these elements, we can generate a trajectory supplying the Cartesian coordinate components of position X, Y, Z, and velocity $\dot{X}$, $\dot{Y}$, $\dot{Z}$ using the iterative method as shown in Section II, Part B.

24

This iterative method applied in a step-wise fashion actually amounts to a numerical integration of equations (63) through (68).

1. Trajectory Generation for Tangential Low-Thrust Circle-to-Circle Orbital Transfers. We can uniquely describe the disturbing function operator ∇R in equation (58) to be a low-thrust tangential force vector $\overline{F}$, where as the solutions of equations (63) through (68) will contain the additional components of acceleration, thereby perturbing Keplerian two-body motion. It is easily shown that starting with an initial circular orbit and initiating a low-thrust force tangent to the orbit, the most profound change occurs in the semimajor axis a. Thus, we can concentrate this analysis, obtaining in explicit form $\frac{\partial R}{\partial M}$ in equation (63) giving us the solution to $\dot{a}$. To expedite this we define

$$\nabla R = \frac{\partial R}{\partial x}\,\overline{i} + \frac{\partial R}{\partial y}\,\overline{j} + \frac{\partial R}{\partial x}\,\overline{k} = \overline{F} \tag{69}$$

where $\overline{F}$ can be explicitly resolved to always lie along the velocity vector by the transformation shown in Figure 3 and the transformation equations (36) through (41). We have then

$$\frac{\partial R}{\partial M} = \nabla R \cdot \frac{\partial \overline{r}}{\partial M} = \overline{F} \cdot \frac{\partial \overline{r}}{\partial M} \tag{70}$$

The explicit form for $\frac{\partial \overline{r}}{\partial M}$ is obtained by using equation (9) and the transformation matrix equation (37). Thus equation (63) finally becomes

$$\dot{a} = \left\{ \frac{2\,[\,r^2\,e^2\,\sin^2\Theta + a^2\,(1-e^2)^2\,]}{r^2\,n\,(1-e^2)^{1/2}\,(1+e^2+2e\,\cos\Theta)^{1/2}} \right\} F_T \tag{71}$$

where F_T is the magnitude of the tangential force. Using equation (10) we have

$$\frac{da}{dt} = \frac{da}{d\Theta}\frac{d\Theta}{dt} = \frac{na^2\,(1-e^2)^{1/2}}{r^2}\frac{da}{d\Theta}$$

We can now transform equation (71) and show a change in the semi-major axis for one revolution of the orbit due to thrusting in a tangential direction:

$$da = F_T \int_0^{2\pi} \left\{ \frac{2[r^2 e^2 \sin^2 \Theta + a^2 (1-e^2)^2]}{r^2 n (1-e^2)^{\frac{1}{2}} (1+e^2+2 e \cos \Theta)^{\frac{1}{2}}} \right\} \left\{ \frac{r^2}{na^2 (1-e^2)^{\frac{1}{2}}} \right\} d\Theta \quad (72)$$

It can be demonstrated that a characteristic of equation (72) is that the effect on Δa of a change in the eccentricity is at most second-order or higher.

Also for tangential low-thrust, eccentricity changes very slowly with time and the $\dot{e}$ equation derived from equation (64) shows that when $e = o$, $\dot{e} = o$. Thus if we set $e = o$ in equation (72) and perform the indicated integral we obtain a Δa for one revolution of the orbit

$$\Delta a = \frac{4\pi}{n^2} F_T \quad (73)$$

Dividing both sides of equation (73) by the period of one orbit we obtain

$$\frac{\Delta a}{\Delta t} = \frac{2 F_T}{n} \quad (74)$$

We, therefore, arrive at a value of $\dot{a}$ for an initial circular orbit and perturb a at selected steps along the orbit. At the end of one revolution, a new $\dot{a}$ is calculated and a is now perturbed at the new rate.

Applying the trajectory generation methods described in Section II, Part B, we compute position and velocity in geocentric Cartesian coordinates while the altitude of the orbit is constantly changing.

2. Atmospheric Drag and Low-Thrust Descent. Atmospheric drag produces the direct opposite effect on Keplerian motion as that produced by a tangential low thrust force along the velocity vector, since the drag force vector is directly opposite the direction of motion.

We thus describe the nature of the drag force vector

$$- F_{T_D} = - \frac{C_D A_b \, \rho V^2}{2m}$$ (75)

where

C_D = drag coefficient

A_b = cross-sectional area of orbiting body

m = mass

V = linear speed

ρ = atmospheric density at a point

$- F_{T_D}$ may be substituted in equation (74) and applied in the previously described method obtaining a value for $-\Delta a$ due to drag.

A conceivable Space Shuttle/Tug mission would be to retrieve a payload from geosynchronous orbit via low-thrust solar electric propulsion. If we direct the thrust vector $\overline{F}_T$ directly opposite the velocity, thus creating a force of magnitude $- |F_T|$, we can lower our orbit to the desired altitude, using previously described techniques for circle-to-circle transfers.

3. First Order Perturbing Effects Due to an Oblate Earth. We may proceed in a like manner by defining the components of the force vector $\overline{F}$ arising from the potential produced by an irregular shaped — nonhomogeneous sphere. The components are resolved as before, relative to the inertial system described in Figure 3.

Using equations (66) and (67), along with previously shown methods, we describe the effects of an oblate earth only on those elements that undergo secular perturbation, thus ignoring the periodic perturbations.

These elements and their first order form are:

$$\dot{\Omega} = \frac{-\frac{3}{2} J_2 \, n \, \cos i}{\left(\frac{a}{R_E}\right)^2 (1-e^2)^2} \qquad (76)$$

and

$$\dot{\omega} = \frac{\frac{3}{2} J_2 \, n \left(2 - \frac{5}{2} \sin^2 i\right)}{\left(\frac{a}{R_E}\right)^2 (1-e^2)^2} \qquad (77)$$

where the earth-zonal harmonic term is $J_2 = 1.0827$ by 10^{-3} and the earth's radius is $R_E = 6378.160$ Km.

It is obvious from equations (76) and (77) that the nodal regression rate and the perigee regression and advancing rates are primarily functions of the inclination of the orbit for purely Keplerian considerations.

The perturbation in the mean anomaly M is compensated for by using a slightly perturbed value of mean motion for Keplerian orbits.

$$\Delta n = \frac{-\frac{3}{2} J_2 \, n}{\left(\frac{a}{R_E}\right)^2 (1-e^2)^{\frac{3}{2}}} \left(\frac{3}{2} \sin^2 i - 1\right) \qquad (78)$$

Thus, the oblate mean motion becomes

$$n^* = n + \Delta n \qquad (79)$$

and the change in the Keplerian period due to the earth's oblateness becomes

28

$$T^* = \frac{2\pi}{n^*} \tag{80}$$

For low thrust trajectory analysis these values are updated after each revolution.

E. Cross-Range/Down-Range Computation

To meet the Space Shuttle vehicle constraints with regards to landing site acquisition opportunities (LSAO), the Space Shuttle Mission Analysis Code computes the instantaneous cross-range and down-range at each point in the program that position is computed.

Performing two of the indicated rotations of Figure 5; i.e., a positive rotation through λ_L and a negative rotation through $-\Phi_L$, a vector is defined pointing to the launch site.

$$\overline{L} = \cos \Phi_L \cos \lambda_L \overline{i} + \cos \Phi_L \sin \lambda_L \overline{j} + \sin \Phi_L \overline{k} \tag{81}$$

Performing two of the indicated rotations of Figure 3; i.e., a positive rotation through Ω^* and a positive rotation through i, a vector perpendicular to the orbital plane is defined.

$$\overline{H} = \sin i \sin \Omega^* \overline{i} - \sin i \cos \Omega^* \overline{j} + \cos i \overline{k} \tag{82}$$

The instantaneous angle from which cross-range is computed becomes

$$\beta^* = \sin^{-1} (\overline{L} \cdot \overline{H}) \tag{83}$$

To compute the instantaneous down-range, a unit vector perpendicular to the plane containing $\overline{L}$ and $\overline{H}$ is computed

$$\overline{N} = \frac{\overline{L} \times \overline{H}}{|\overline{L} \times \overline{H}|} \tag{84}$$

Now, the projection of $\bar{L}$ on the orbital plane is given by

$$\bar{P} = \bar{H} \times \bar{N} \tag{85}$$

An instantaneous vehicle position in the orbital plane $R(X, Y, Z)$ is computed as described in Section II, Part B.

The instantaneous down-range angle which gives the relative position of the spacecraft in the orbital plane to the projection of the launch site vector on the orbital plane is thus

$$\Theta^* = \cos^{-1}(\bar{R} \cdot \bar{P}) \quad . \tag{86}$$

F. Space Radiation Analysis

Since electrons and protons are magnetically trapped about the earth, a representation of their distribution may be made based on the contours of the magnetic field lines and the magnetic field strength at a point in space. This was accomplished by using the B-L coordinate system developed by Carl McIlwain [10], as depicted in Figure 6. The B coordinate denotes the magnetic field strength at a specified point in space and the L coordinate is the magnetic shell parameter that specifies the shell upon which the guiding center of the trapped particles is confined as it drifts around the earth. The L coordinate is approximately constant along a geomagnetic field line.

Essentially, a three-dimensional space of latitude, longitude and altitude is transformed into a two-dimensional space of B and L which serves to more expediently construct a model radiation environment based on this method.

For the proton environment, the omnidirectional integral flux spectrum may be represented by

$$J(>E, BL) = F(B, L)e^{\frac{E_1 - E}{E_o(B, L)}} \tag{87}$$

where E_1 to E is the particular energy band of interest and E_o is a spectrum-shaping parameter and a function of B and L. $F(B,L)$ is the known intensity of the proton flux for a given energy at a specific point. Equation (87) then defines the integral spectrum on the integral number of particles greater than E_1 in the spectrum.

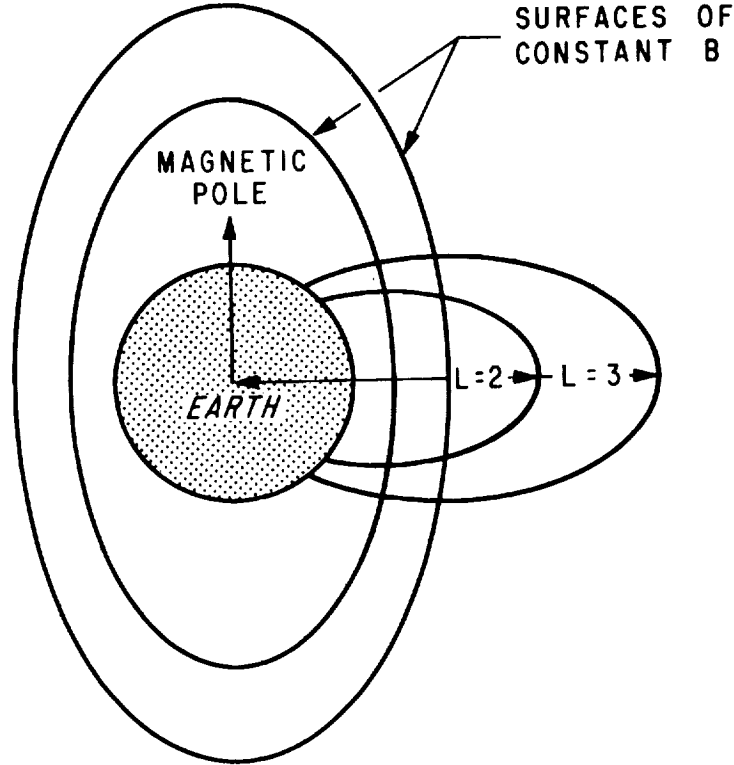The units of J are protons/cm²-sec.

Figure 6. Geometry of the B-L coordinate system.

To obtain the differential energy spectrum which gives the number of particles at specific energies in the spectrum, we differentiate equation (87) with respect to E and obtain

$$- J'(E,B,L) = \frac{F(B,L)}{E_o(BL)} \; e^{\frac{E_1 - E}{E_o(B,L)}} \tag{88}$$

where the units of J' are protons/cm²-sec-meV.

31

A differential and integral spectrum may then be completed for any point in the space model. However, for a typical Space Shuttle Mission, time-averaged calculation may be of greater interest.

The Space Shuttle Mission Analysis Code calculates this time-averaged data for magnetically trapped protons in the following manner: a proton flux $F[B(t), L(t)]$ is computed at each orbital step of 5 deg, which may vary, of true anomaly for an entire 7-day mission.

From equation (87) we may compute this time averaged, or mean value, of the proton flux $> E_1$ as

$$\bar{J}(>E) = \frac{1}{t_n - t_o} \int_{t_o}^{t_n} F[B(t), L(t)] e^{\frac{E_1 - E}{E_o[B(t), L(t)]}} dt \qquad (89)$$

When $E = E_1$ equation (89) takes the form

$$\bar{J}(>E_1) = \frac{1}{t_n - t_o} \int_{t_o}^{t_n} F[B(t), L(t)] dt \qquad (90)$$

which gives a time-weighted average of all the partials in the spectrum greater than the specified energy E_1. Now, instead of choosing a representative spectrum at a single point, a representative average spectrum is chosen based on the spacecraft's encounter with the radiation environment during the entire mission. From equation (88) we also have the time averaged differential energy spectrum for a Space Shuttle Mission with a time duration of t_o to t_n.

$$\bar{J}(E) \quad \frac{1}{t_n - t_o} \int_{t_o}^{t_n} \frac{F(B, L)}{E_o[B(t), L(t)]} e^{\frac{E_1 - E}{E_o[B(t), L(t)]}} dt \qquad (91)$$

where the units of J are as previously indicated.

A similar analyses with some variation is performed to model the magnetically trapped electron environment.

G. Program Implementation — Start/Stop — Input/Output Control Options

1. Generation of Starting State Vector. The Space Shuttle Mission Analysis Code requires as initial input a starting state vector specifying the initial orbit along with an associated ground elapsed time (g.e.t.) since lift-off or g.e.t. since initial orbit insertion. This state vector takes the form of a set of geocentric orbital elements or other initial condition information defined in Section II, Part C. If planar flight is assumed during ascent, the code will generate its own starting state vector based on the following information.

a. Launch site geocentric latitude and longitude.

b. Orbit insertion geocentric latitude and longitude for the initial Shuttle base line orbit.

c. Launch or insertion azimuth or the inclination of the desired orbit.

d. The desired final altitude for on-orbit operations and the conducting of experiments.

It is apparent then, that the method of obtaining the starting state vector will depend upon the kind of information available and other characteristics of the ascent portion of the Space Shuttle flight.

2. Specific Start/Stop Program Control Options. Once the starting state vector has been defined, the following starting and run time control options are available:

a. The ability to start the analysis at any time into the mission; i.e., it may be desirable to perform only deorbit and reentry analyses at the end of a seven-day mission.

This means also that any segmented portions of a mission may be analyzed for any desired time increments. For example, such an analysis may be required to define all the possible landing site acquisition opportunities during the entire mission.

b.   Designating a mission time cutoff or specifying the number of revolutions desired as a means of terminating the analysis of a specific mission.

c.   A continuous unsegmented analysis of mission parameters from insertion into the operational orbit through deorbiting and the achieving of specified reentry constraint conditions (defined later).

3.   Rendezvous Analysis Output.   Space Shuttle Mission Analysis Code provides the following output parameters to expedite rendezvous analysis:

a.   A complete ground trace of the spacecraft's trajectory from orbit insertion through the deorbit maneuver to the reentry target point.

Two advantageous features of the ground trace computational techniques are, (1) there is no dependence on knowing the relative position of the vernal equinox with respect to Greenwich as a function of time and, (2) the code employs a tracking technique which constantly updates those orbital elements that undergo secular perturbations due to first order oblate spherical terms and the rotational motion of the earth, thus eliminating the need for separate time-consuming integration techniques.

b.   The position and the velocity of the spacecraft in any desired time increments defined in geocentric rectangular coordinates (X, Y, Z) and spherical coordinates (γ, Φ, λ).

c.   Orbital Maneuvering System (OMS) ΔV requirements for coplanar transfer and circularization maneuvers including phasing and retrograde deorbiting.

d.   Time into the mission associated with each event using the initial insertion time or g.e.t. since lift-off as the zero time reference.

e.   Nodal regression rates and perigee procession or regression rates along with the instantaneous nodal crossing.

Rendezvous Analysis involving two vehicles is accomplished by, (1) running the target vehicle's trajectory, (2) modifying it if necessary using phasing orbits to change the original ground track to the desired ground track, (3) running the pursuit vehicle's trajectory starting with an initial state vector based on an instantaneous set of orbital elements defined from the target vehicle's trajectory, and (4) adjusting the pursuit vehicle's lift-off time and phasing altitude to insure a desired initial-phasing angle that corresponds with the desired rendezvous and docking time and position.

There is no automatic optimization techniques inherent in the Space Shuttle Mission Analysis Code; however, an optimum, or most economical, rendezvous sequence is arrived at through the operator's analysis of various pursuit and target vehicles parameters and trajectories.

4. Reentry Analysis Output. As was stated earlier, the Space Shuttle Mission Analysis considers all space a vacuum, therefore reentry analysis does not attempt to define the spacecraft's trajectory through the atmosphere proper. The code, however, does define certain reentry constraint conditions and shows the time into the mission when all these conditions are met for successful Landing Site Acquisitions Opportunities (LSAO). Specifically the output includes:

a. A complete deorbit profile from which any desired reentry angle into the earth's atmosphere may be chosen (usually a range from 0.0 to -2.0 because of vehicle heating constraints).

b. The position and velocity of the spacecraft at the reentry target altitude as a function of the particular angle of reentry and the altitude at which deorbit retro fire was initiated. A single reentry angle may be chosen to expedite a faster run time and less data print-out.

c. Instantaneous vehicle cross-range and down-range distances to landing site during the entire mission, which is used to determine at what time deorbit maneuvers may occur to allow for a successful LSAO.

d. A running abbreviated deorbit profile (having a suppressed range of parameters) for possible mission aborts, which outputs all reentry constraint information as a function of deorbiting (retrograde) at any point of any circular orbit during the entire mission. This unique feature of the Code is accomplished by the periodic or cyclic rotation of the deorbit conic to coincide with whatever position in orbit that the spacecraft happens to be.

e. The deorbit trajectories in Cartesian (X, Y, Z) and spherical coordinates (γ, Φ, λ) defined as a function of the particular angle of reentry chosen. Included in this output is the time of flight from deorbit retro firing to the atmospheric reentry target altitude which is also a function of range of reentry angles considered.

f. Orbital Maneuvering System ΔV requirements for retrograde deorbiting, also a function of desired reentry angle and altitude of deorbit initiation. There is no restriction here to circular orbits. However, when deorbiting occurs from other than a circular orbit it occurs at the apogee point of the orbit.

Again there is no attempt at automatic optimization, but an output which includes a full range of mission and vehicular constraint data enables the user to easily define all acceptable conditions of reentry, including the optimum ones.

5. Radiation Analysis Output. Space Shuttle Mission Analysis Code performs a comprehensive analysis of the space radiation environment of magnetically trapped electron and protons encountered on a specific Space Shuttle Mission. The analysis included in this document was performed with the latest available environmental data; however, this data is periodically updated as new radiation environment models are defined and distributed. The output of this portion of the code includes:

a. The differential and integral energy spectra for magnetically trapped electrons and protons as a function of spatial coordinates.

b. A time-averaged differential and integral energy spectrum for protons and electrons as a function of mission time; i.e., after any integral number of orbits or for the entire mission.

c. Total number of particles above a specified energy encountered on a particular mission.

d. Flux intensities for electrons and protons at any defined point in space thus defining the particular configuration of the model environment as a function of particle energies.

These time averaged energy spectra may then be used to calculate radiation doses, including crew skin doses, by transporting them through certain thicknesses of materials using available nuclear radiation transport and dose calculation codes.

6. General. The Space Shuttle Mission Analysis computer program was coded in Fortran IV — Double Precision, and currently runs on the IBM 7044 computer. Since computer run time is greatly affected by the print-out option, the program source decks are now in three parts. Rendezvous and Reentry Analysis comprise a single deck requiring approximately 12 000 core storage locations. Radiation Analysis (Electrons) and Radiation Analysis (Protons) comprise two separate program source decks, each requiring approximately 26 000 core storage locations.

Print-out suppression options are available when less information is desired, thereby greatly decreasing the amount of computer run-time required.

SECTION III. APPLICATIONS (COMPUTATIONAL RESULTS, TASK 1, 2, AND 3)

The primary purpose of this section is to demonstrate the appli- cations of the Space Shuttle Mission Code to perform Space Shuttle Mission Analyses using realistic and probable missions. Rendezvous, radiation and reentry analysis has been performed for four typical Space Shuttle Missions. The presented data also includes a parametric study on single impulse versus double impulse deorbiting ΔV requirements for the Space Shuttle Orbiter which may be considered general reference data.

A. Task 1 — Two Dimensional Reentry Analysis

The first study undertaken was to show the relative orbital maneuvering system ΔV requirement for single impulse versus double impulse deorbit maneuvers when the Space Shuttle orbiter is operating at relatively low alti- tudes and reentering the atmosphere over the range of angles from 0.0 to -2.0 deg. The range of reentry angles is dictated by vehicle heating constraints. It was discovered that, for specific angles within this range, the ΔV requirement for single impulse deorbit was considerably higher than the ΔV requirement for double impulse deorbit when the spacecraft is operating at altitudes below 400 Km. Thus, it is more economical to transfer to a higher orbit before deorbiting for reentry when the reentry angle is within the applicable range.

Figures 7 through 10 show the relative ΔV requirements for single impulse versus double impulse deorbit maneuvers at various orbiter altitudes and achieving the indicated range of atmospheric reentry angles.

Using the "arrowed" single impulse line as a reference, all double impulse readings above the line represent a ΔV saving for double impulse maneuvers, and all double impulse readings below the reference line represent a ΔV penalty paid for performing the double impulse maneuver and achieving the indicated range of atmospheric reentry angles.

Figures 9 and 10 show that as the initial circular orbit increases in altitude, little or no ΔV savings occur by performing a double impulse maneuver over the range of considered atmospheric reentry angles.

Figure 11 shows the relative velocities that the spacecraft would have at the reentry target altitude of 120.38 Km (65 N. Mi.) after specified transfer maneuvers and reentering the atmosphere within the designated range of reentry angles.

Figure 7. ΔV requirement for transfer from initial
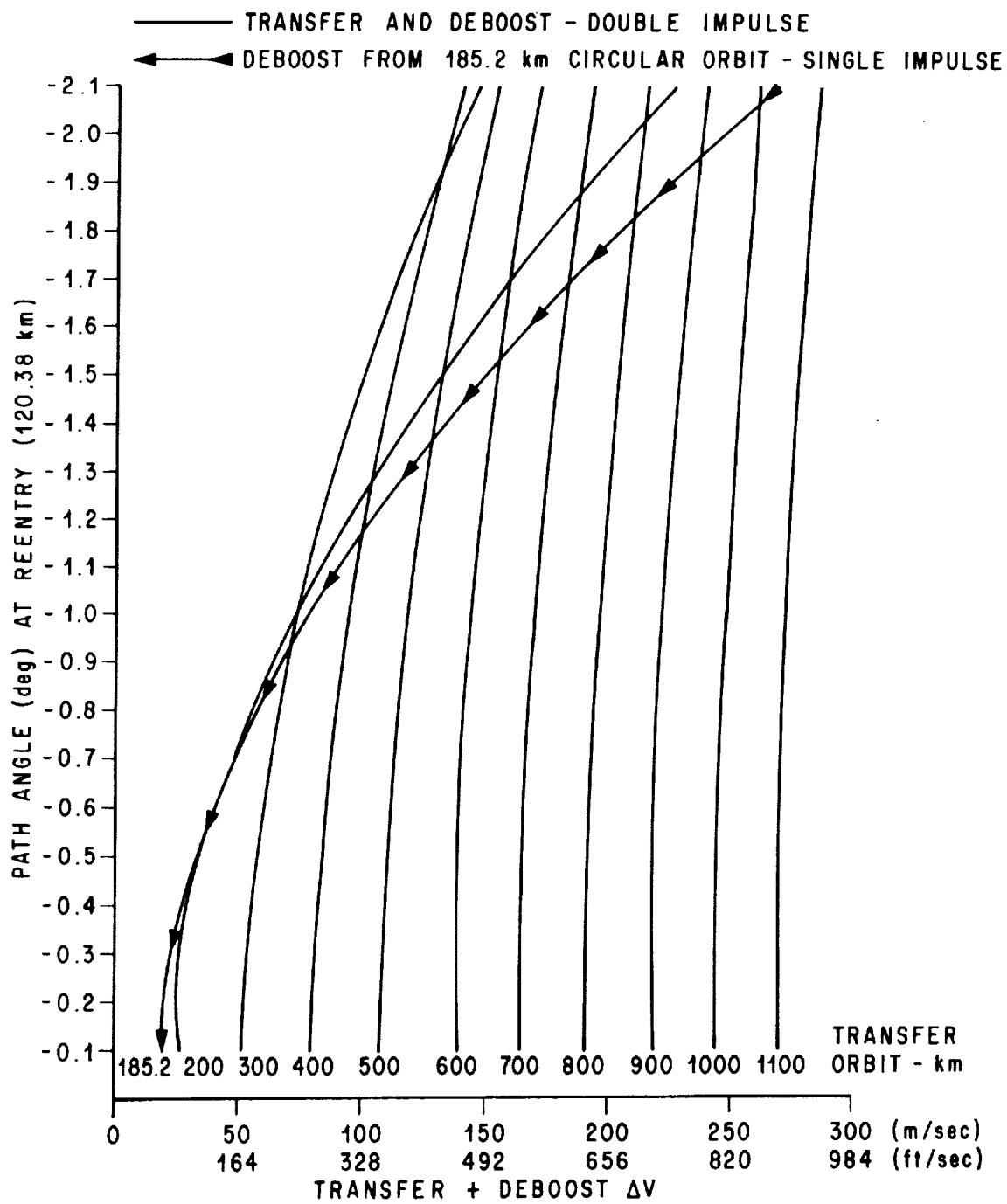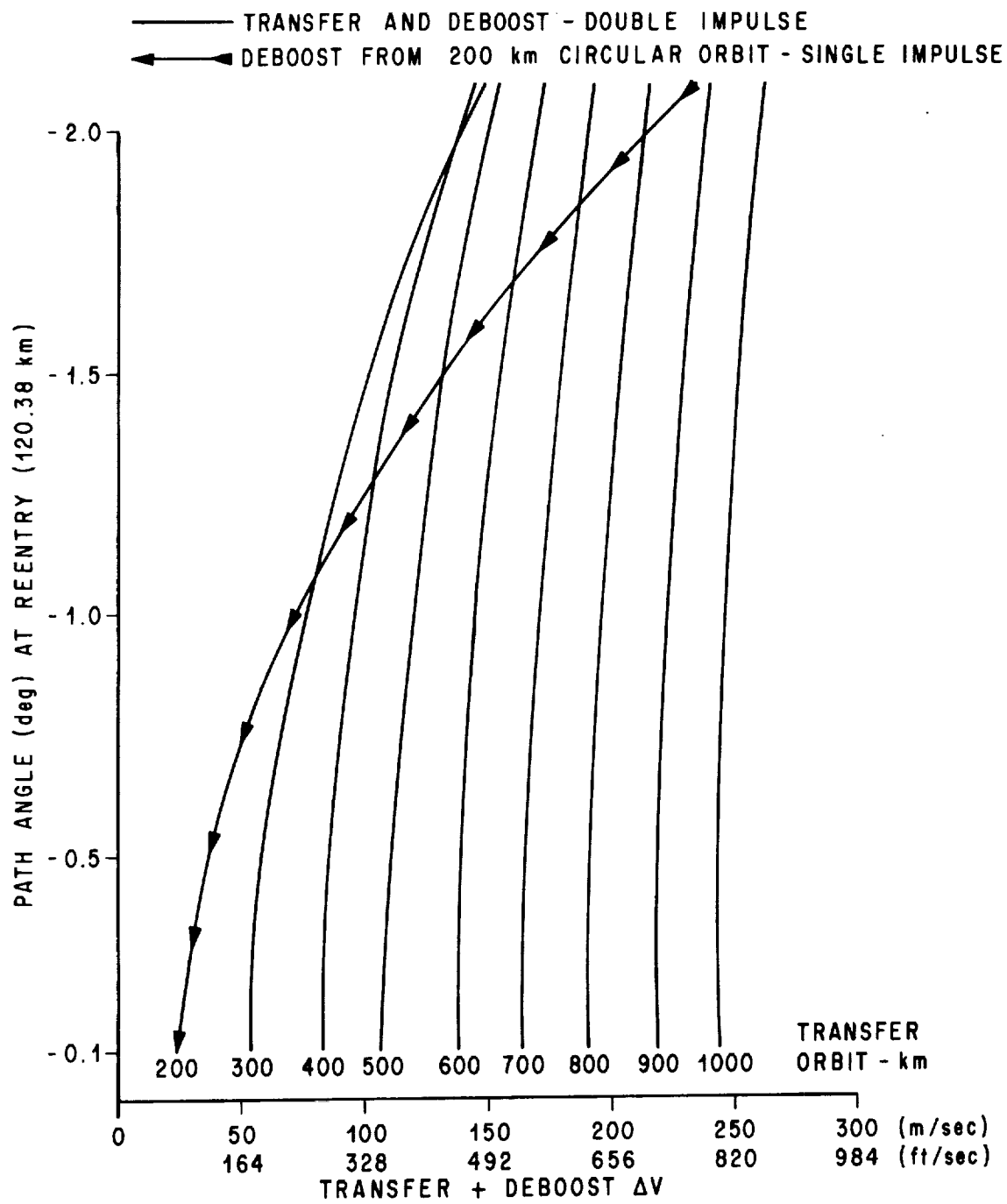185.2 km circular orbit and deboost.

38

Figure 8. ΔV requirement for transfer from initial
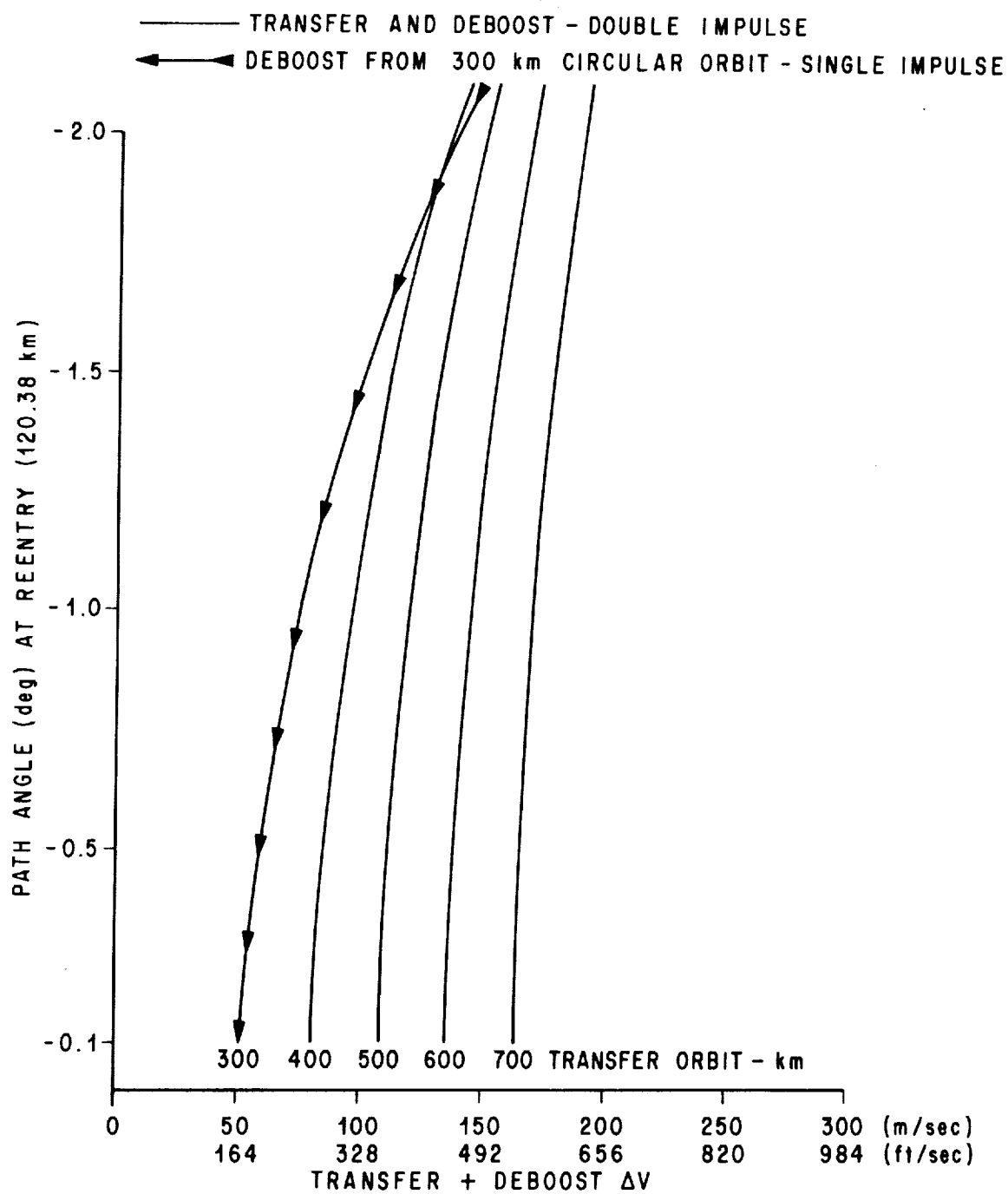200 km circular orbit and deboost.

39

Figure 9. ΔV requirement for transfer from initial
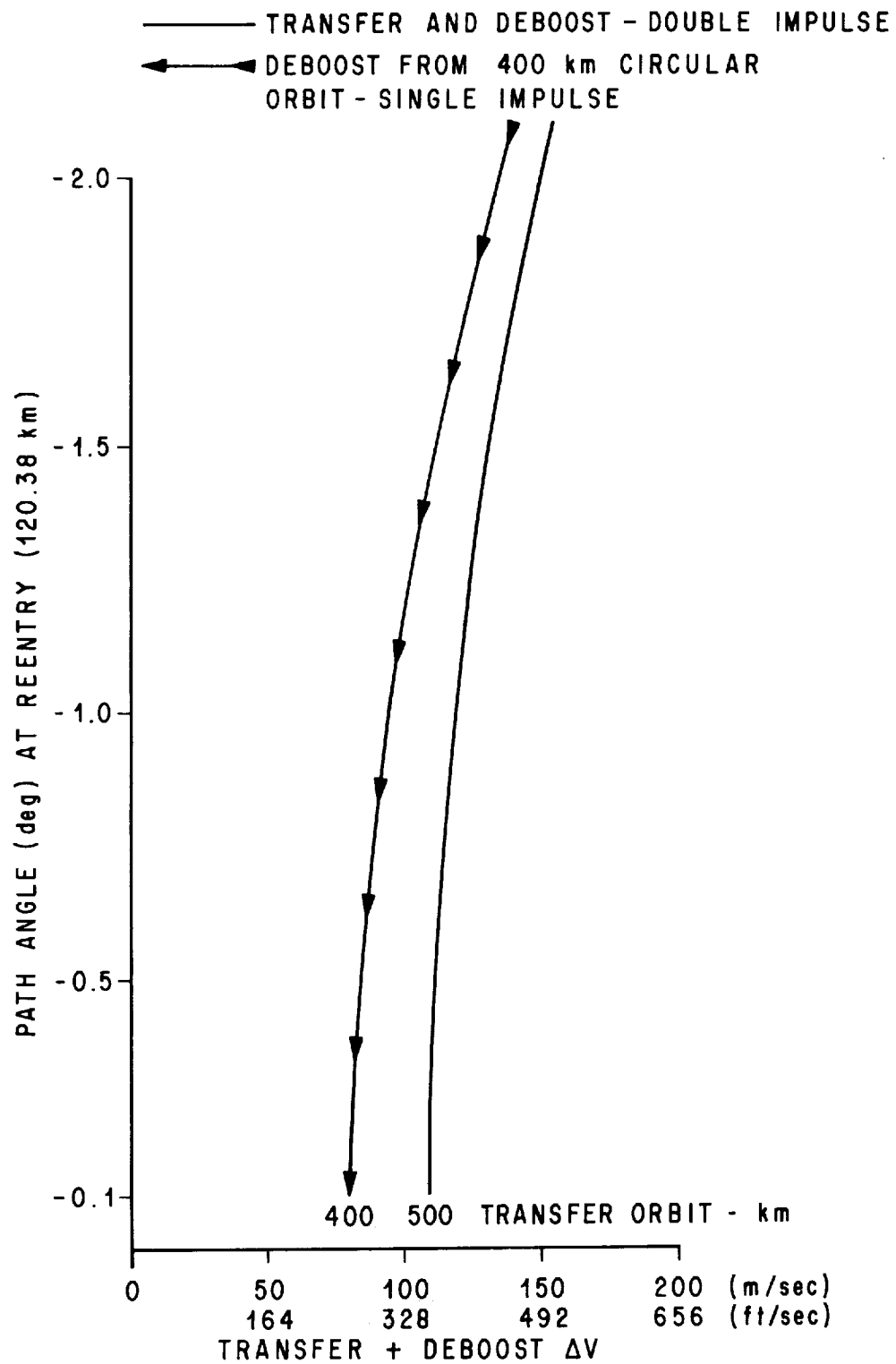300 km circular orbit and deboost.

40

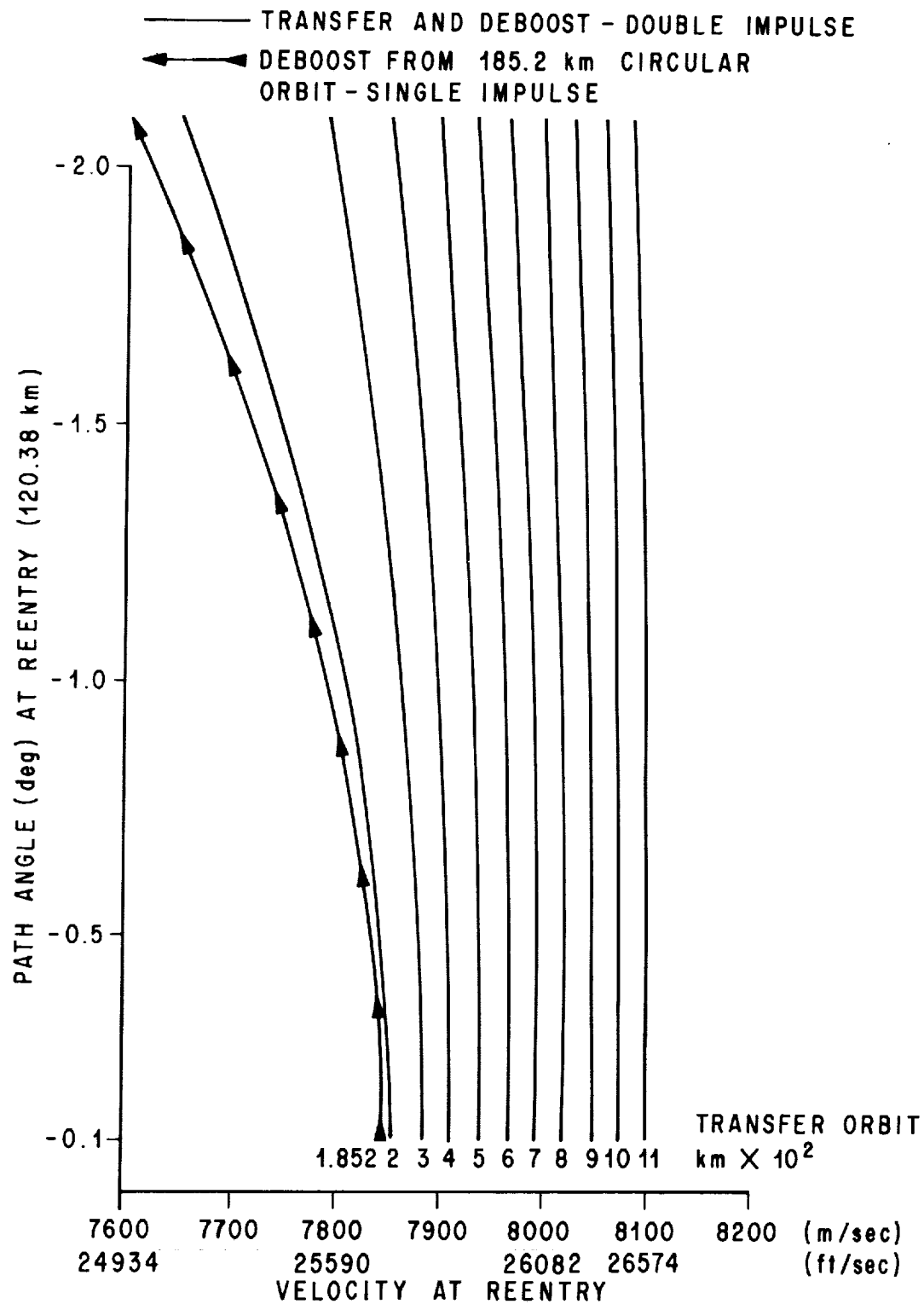Figure 10. ΔV requirement for transfer from initial
400 km circular orbit.

Figure 11. Reentry velocity after transfer and deboost
from initial 185.2 km circular orbit.

42

B. Task 2 — Three-Dimensional Rendezvous and Reentry Analysis

Task 2 demonstrates the versatility and flexibility of the Space Shuttle Mission Analysis Code to perform three-dimensional mission analysis for Space Shuttle Missions covering a wide range of orbital parameters.

The illustrated computational results will show a ground trace of the orbiter from insertion into the operational orbit through the deorbit maneuver including the deorbit trajectory and the arrival of the orbiter at a reentry target altitude, meeting a predetermined set of reentry constraints.

Variation in the set of reentry constraint conditions has little or no bearing on the analysis of a particular mission, since a wide-enough range of instantaneous reentry constraint data is an output of each mission analyzed. One has only to define this set for a particular mission.

Unless otherwise noted, the particular set of reentry constraint conditions, which assures successful landing site acquisition opportunities (LSAO) for the simulated missions presented herein, are as follows:

(1) 4475 ≤ down-range ≤ 6475 n. mi.

(2) 0.0 n. mi. ≤ cross-range ≤ 1100 n. mi. (east or west).

(3) Reentry angle = -1.31 deg (Mission One) and -1.35 deg (Mission Two).

(4) Reentry velocity = 25693 ft/sec (Mission One) and 25845 ft/sec (Mission Two).

(5) Maximum 7 day mission duration time.

1. Example Space Shuttle Mission One (Earth Resources). The first example mission chosen is a projected earth resources technology Sortie Lab mission. Orbital parameters are chosen to provide maximum viewing time during daylight hours of the Chesapeake Bay region with an approximate center of 38.0 deg altitude and -76.0 deg longitude.

The orbit altitude is 268.54 km (145 n. mi.) and is an approximate daily repeating orbit with an inclination of 89.73 deg. The launch and landing site is the Western Test Range (WTR), Vandenberg Air Force Base, California.

Table 1 shows the sequence of flight events for the mission from insertion into the initial 50-by-100 n. mi. orbit to the achieving of the final set of reentry conditions as defined earlier. The specific LSAO for Mission One aborts and mission completion would meet the defined reentry constraints. Timelining information is also a feature of Table 1.

TABLE 1. TYPICAL SPACE SHUTTLE MISSION ONE (ERTS)

SEQUENCE OF FLIGHT EVENTS

Event	Time[a] of Initiation (Sec)	Δ Time to Next Event (Sec)	Propulsion System	Event ΔV, m/s (fps)	Resultant ha/hp km (n. mi.)	Position Latitude (deg)	Longitude (deg)	Altitude km (n. mi.)
Insertion into initial orbit of 50 by 100 n. mi.	0.0	2617.9	NA	NA	185.2 by 92.6 (100 by 50)	20.15	-121.59	92.6 (50)
First Impulsive burn	2617.9	2643.2	OMS	27.58 (90.5)	185.2 by 185.2 (100 by 100)	-20.02	47.15	185.2 (100)
Second Impulsive burn	5261.1	2671.1	OMS	24.54 (80.5)	268.54 by 185.2 (145 by 100)	19.89	-144.14	185.2 (100)
Third Impulsive burn (circularization)	7932.2	30282.6	OMS	24.47 (80.3)	268.54 by 268.54 (145 by 145)	-19.75	24.90	268.54 (145)
First LSAO[b] 6th revolution deorbit	38214.8	5396.9	OMS	89.35 (293.16)	268.5 by 0.0 (145 by 0)	-21.43	78.54	268.54
						-70.14	-108.50	120.38
Second LSAO 7th revolution deorbit	43611.71	30882.1	OMS	89.35 (293.16)	268.5 by 0.0 (145 by 0)	-21.70	55.99	268.54
						-69.88	-131.08	120.38
Begin first pass over Chesapeake Bay — 13th revolution	74493.8	899.5	NA	NA	268.5 by 268.5 (145 by 145)	76.61	-74.26	268.54 (145)
End first pass over Chesapeake Bay	75383.3	7645.6	NA	NA	268.5 by 268.5 (145 by 145)	16.66	-76.96	268.54 (145)
Third LSAO 14th revolution deorbit	83038.9	5396.9	OMS	89.35 (293.16)	268.5 by 0.0 (145 by 0)	-46.50	-70.87	268.54
						41.99	65.89	120.38
Fourth LSAO 15th revolution deorbit	88435.8	36129.2	OMS	89.35 (293.16)	268.5 by 0.0 (145 by 0)	-46.23	49.33	268.54
						42.26	43.35	120.38
Fifth LSAO 22nd revolution deorbit	124565.0	5396.9	OMS	89.35 (293.16)	268.5 by 0.0 (145 by 0)	-25.73	78.00	268.54
						-65.84	-109.3	120.38
Sixth LSAO 23rd revolution deorbit	129961.9	30882.2	OMS	89.35 (293.16)	268.5 by 0.0 (145 by 0)	-26.00	55.40	268.54
						-65.38	-131.89	120.38
Begin second pass over Chesapeake Bay — 29th revolution	160844.1	899.5	NA	NA	268.5 by 268.5 (145 by 145)	72.31	-74.79	268.54 (145)
End second pass over Chesapeake Bay	161743.5	7647.4	NA	NA	268.5 by 268.5 (145 by 145)	12.35	-77.76	268.54 (145)

44

TABLE 1. (Concluded)

SEQUENCE OF FLIGHT EVENTS

Event	Time[a] of Initiation (Sec)	Δ Time to Next Event (Sec)	Propulsion System	Event Δv, m/s (fps)	Resultant ha hp km (n. mi.)	Position Latitude (deg)	Position Longitude (deg)	Position Altitude km (n. mi.)
Seventh LSAO 30th revolution deorbit	169 390.9	5 396.8	OMS	89.35 (293.16)	268.5 by 0.0 (145 by 0)	-42.20	70.30	268.54
						46.29	65.00	120.38
Eighth LSAO 31st revolution deorbit	174 787.7	36 127.5	OMS	89.35 (293.16)	268.5 by 0.0 (145 by o)	-41.93	47.80	268.54
						46.56	42.55	120.38
Ninth LSAO 38th revolution deorbit	210 915.2	5 396.9	OMS	89.35 (293.16)	268.5 by 0.0 (145 by 0)	-30.03	77.47	268.54
						-61.54	-110.1	120.38
Tenth LSAO 39th revolution	216 312.1	30 882.1	OMS	89.35 (293.16)	268.5 by 0.0 (145 by 0)	-30.30	54.87	268.54
						-61.28	-132.78	120.38
Begin third pass over Chesapeake Bay (45th revolution)	247 194.2	899.5	NA	NA	268.5 by 268.5 (145 by 145)	68.00	-75.43	268.54 (145)
End third pass over Chesapeake Bay	248 093.7	7 647.4	NA	NA	268.5 by 268.5 (145 by 145)	8.04	-78.56	268.54 (145)
NOTE:	Passes over target area occur in multiples of 86 350.2 sec or multiples of 16 revolutions and last for approximately 899.5 sec. LSAO events which last for 2 revolutions consecutively occur in multiples of 43175.1 sec or 8 revolutions (see LSAO figures for details)							
Begin seventh and last pass over Chesapeake Bay	592 145.4	899.5	NA	NA	268.5 by 268.5 (145 by 145)	80.75	-77.81	268.54 (145)
End seventh and last pass over Chesapeake Bay	593 044.8	8 095.4	NA	NA	268.5 by 268.5 (145 by 145)	20.79	-80.02	268.54 (145)
seven-day mission complete 110th revolution deorbit meeting constraints	601 140.2	1318.0	OMS	89.35 (293.16)	268.5 by 0.0 (145 by 0)	-20.66	66.15	268.54 (145)
Orbiter at 394 947.5 ft, reentry angle —1.31 velocity 25 693 ft/sec	602 458.2	TBD	NA	NA	268.5 by 0.0 (145 by 0)	67.83	61.41	120.38 (65)
Landing	TBD	NA	NA	NA	NA	34.536	-120.567	0

a. time = elapsed second since insertion into 50 by 100 n. mi. orbit
b. revolutions = number of orbits since insertion into 145 by 145 n. mi. circular orbit

Notes: (1) altitude: 268.54 km (145 n. mi.)
(2) time of launch for daylight passes over target
(3) inclination: 89.73 degrees
(4) launch azimuth: 182.0 degrees
(5) orbit selection: a 1-day repeating, near polar orbit insuring passes over the Chesapeake Bay region with approximate center of 38.0 deg latitude and -76.0 deg longitude
(6) launch site WTR

Figures 12, 13 and 14 show the ground trace of the first 16 revolutions of the orbiter from circular orbit insertions at point A of Figure 12. Since the orbit is an approximate repeating one, the revolutions essentially represent the complete ground trace for the whole mission.

Figure 15 illustrates at what points above the earth (geocentric latitude Φ and longitude λ) retrograde deorbiting must occur for the indicated revolution numbers in order to meet the previously defined reentry constraints for both mission abort and mission completion reentry conditions.

Figure 16 shows the remaining landing site acquisition opportunities meeting defined reentry constraints.

2. **Example Space Shuttle Mission Two (Advanced HEAO Delivery).** For Space Shuttle Mission Two, all orbit parameters including the launch and landing site will differ from those of Mission One. The Space Shuttle will be launched from the Eastern Test Range, Florida. The operational altitude will be 200 n. mi. and the inclination will be 28.5 deg, due-east launch.

Table 2 gives the sequence of flight events and the Orbital Maneuvering System ΔV requirement for each maneuver performed to get on station and to deorbit. All LSAO are tabulated, meeting the previously defined mission and reentry constraint conditions for Mission Two.

Figure 17 shows the ground trace of the Orbiter from insertion into the 200 n. mi. circular orbit at point A for the first 16 revolutions.

3. **Example Space Shuttle Mission Three (COMM/NAV Geosynch Development).** Example Space Shuttle Mission Three requires a kickstage or tug to place a Communication/Navigation (COMM/NAV) satellite in a geosynchronous 35786.1 km orbit with the option of achieving different positions along a longitudinal shift. The orbit parameters for the Space Shuttle will be essentially the same as for Mission Two; thus the LSAO will remain the same. From a final circular orbit of 200 n. mi., the Space Shuttle will serve as a launch pad for final deployment of the COMM/NAV payload by a delta kickstage to the desired geosynchronous position.

Table 3 gives the sequence of flight events along with the relative time increments for kickstage firing to achieve the desired hovering point in geosynchronous orbit.
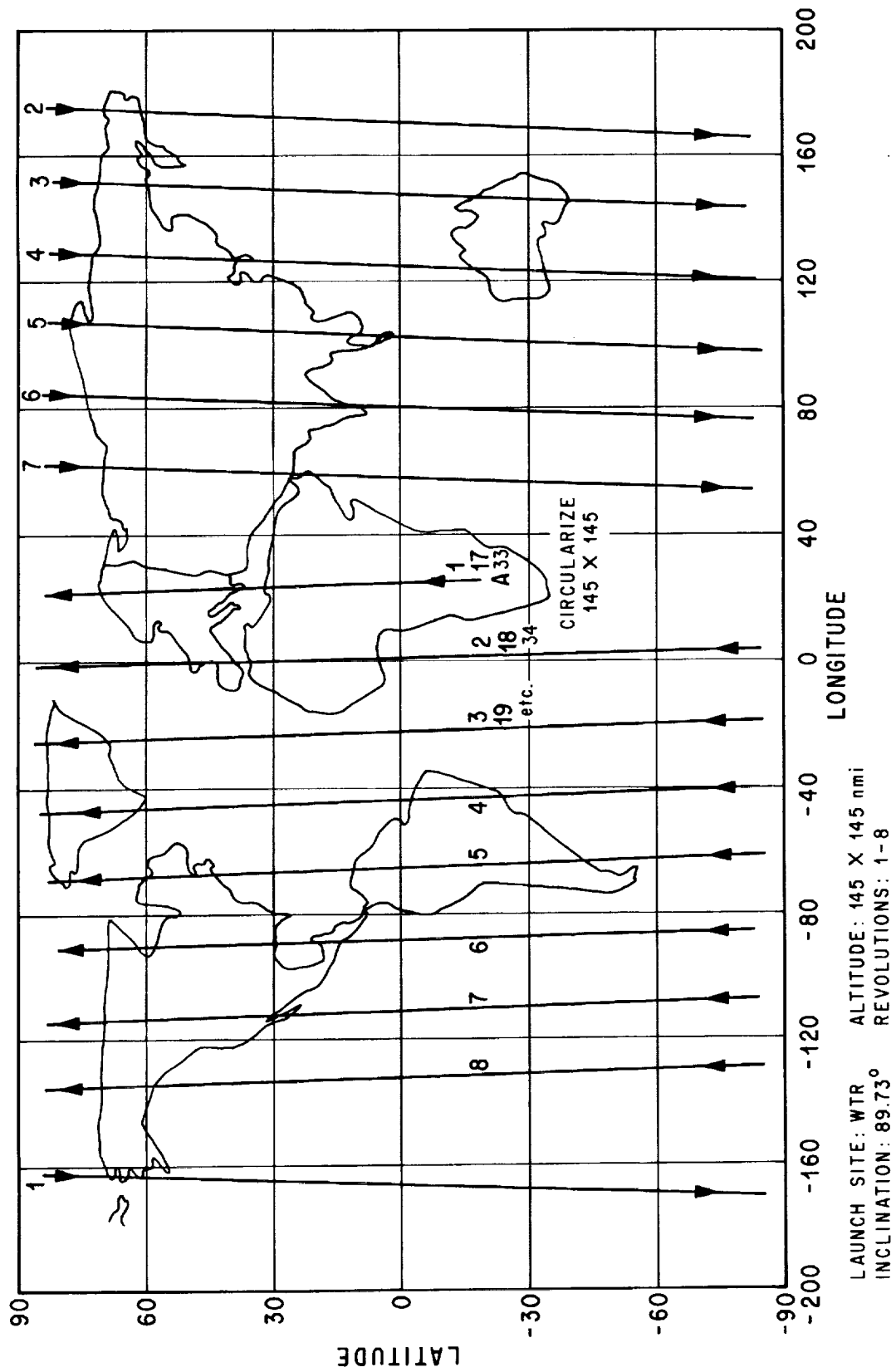
Figure 12. Typical Space Shuttle Mission One (ERTSL) revolutions 1-8.

LAUNCH SITE: WTR   ALTITUDE: 145 X 145 nmi
INCLINATION: 89.73°   REVOLUTIONS: 1-8

47
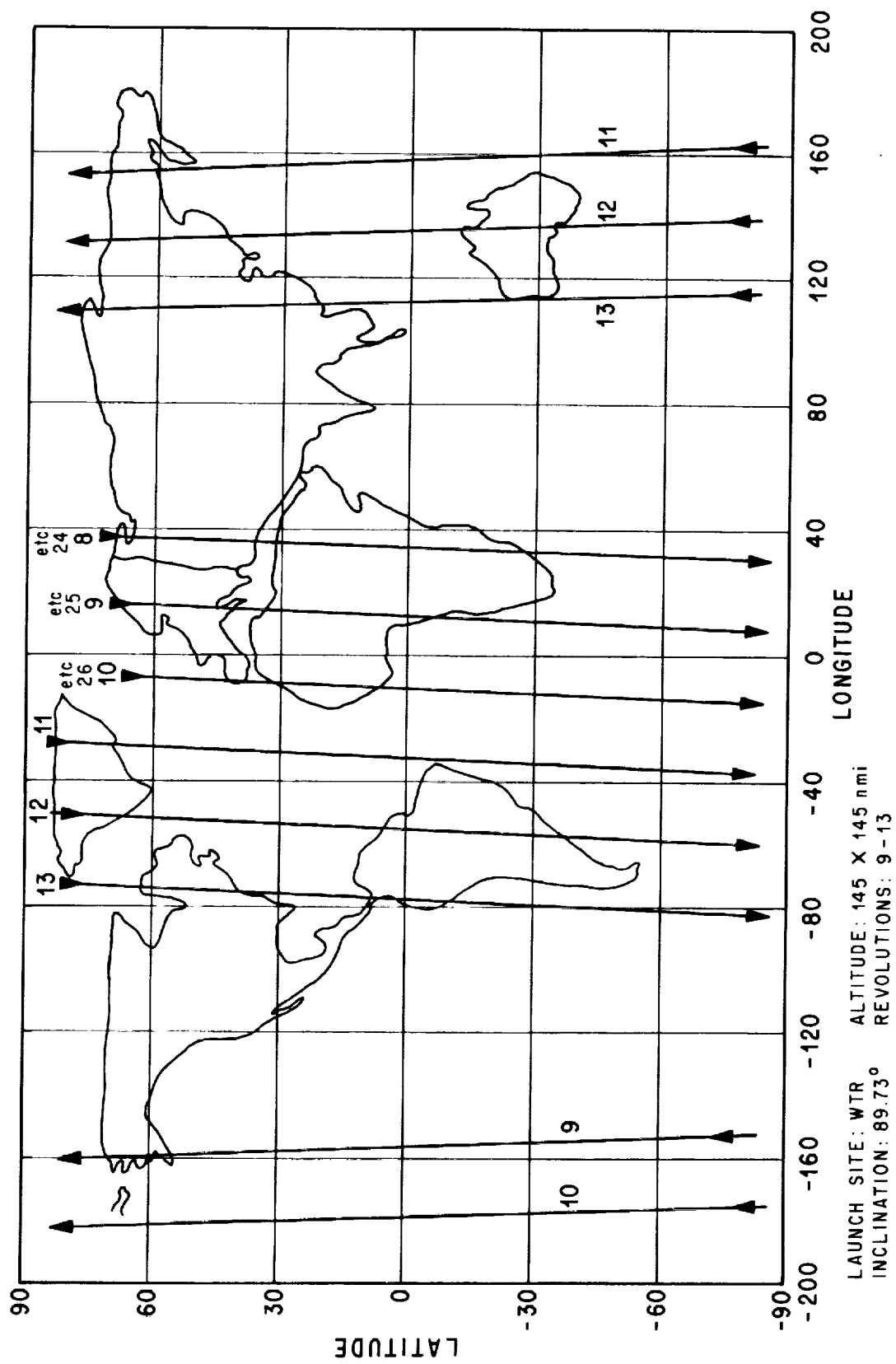
Figure 13. Typical Space Shuttle Mission One (ERTSL) revolutions 9–13.

LAUNCH SITE: WTR   ALTITUDE: 145 X 145 nmi
INCLINATION: 89.73° REVOLUTIONS: 9–13

48
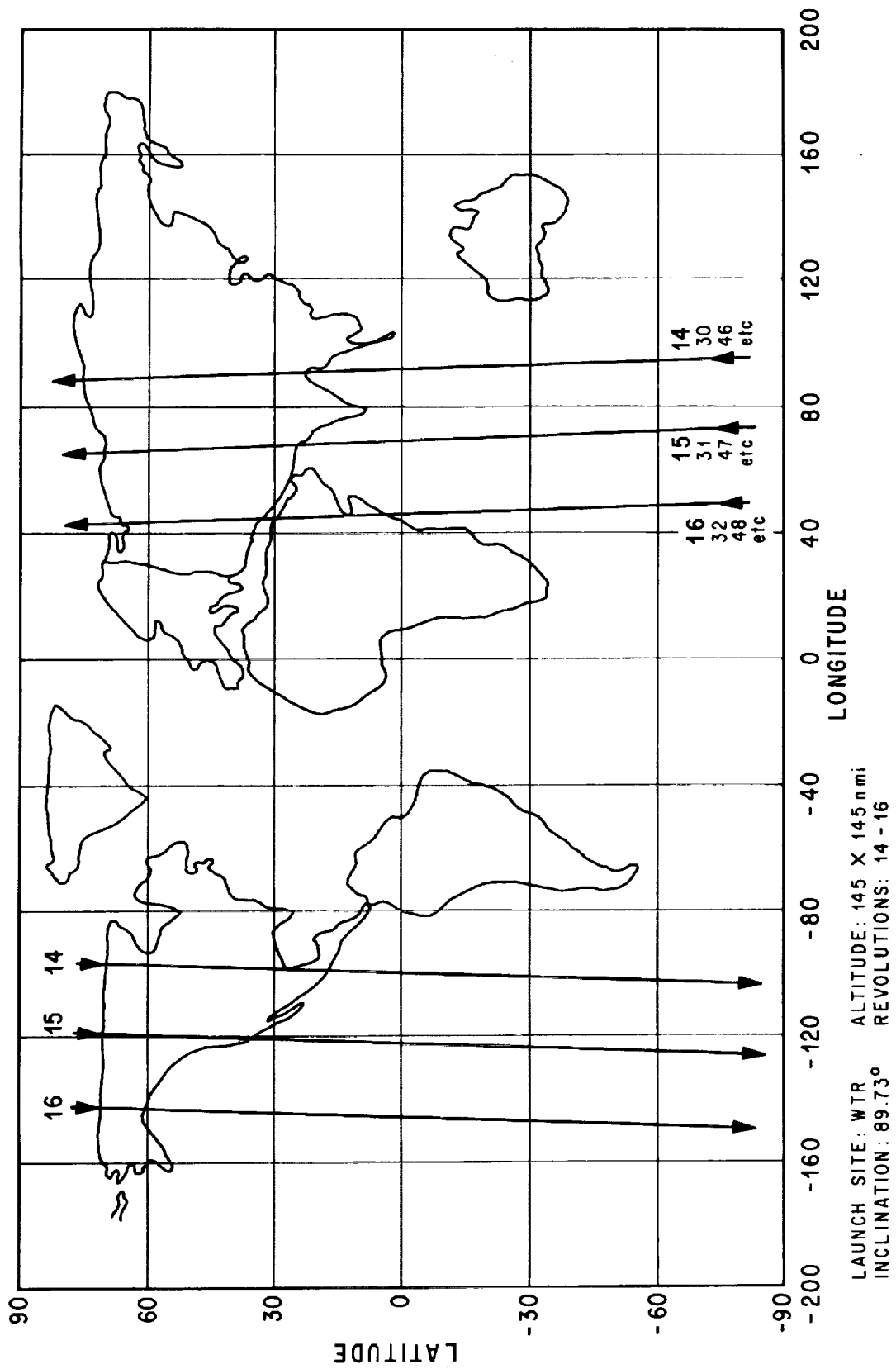
Figure 14. Typical Space Shuttle Mission One (ERTSL) revolutions 14–16.

LAUNCH SITE: WTR   ALTITUDE: 145 X 145 n mi
INCLINATION: 89.73°   REVOLUTIONS: 14 – 16

LONGITUDE

LATITUDE

Figure 15. Typical Space Shuttle Mission One (ERTSL).

50

LANDING SITE ACQUISITION OPPORTUNITIES (LSAO) MEETING THE FOLLOWING REENTRY CONSTRAINTS:

(1) 4475 nmi ≤ DOWNRANGE ≤ 6475 nmi
(2) 0 nmi ≤ CROSSRANGE ≤ 1100 nmi (EAST OR WEST)
(3) 7 DAY MISSION DURATION

(4) REENTRY ANGLE = -1.31° } AT 394,947.5 ft
(5) REENTRY VELOCITY = 25693 ft/sec } (65 nmi)

LAUNCH SITE: WTR   INCLINATION: 89.73°
LANDING SITE: WTR   ALTITUDE: 145 X 145 nmi
LAUNCH AZIMUTH: 182.0°

Figure 16. Typical Space Shuttle Mission One (ERTSL).
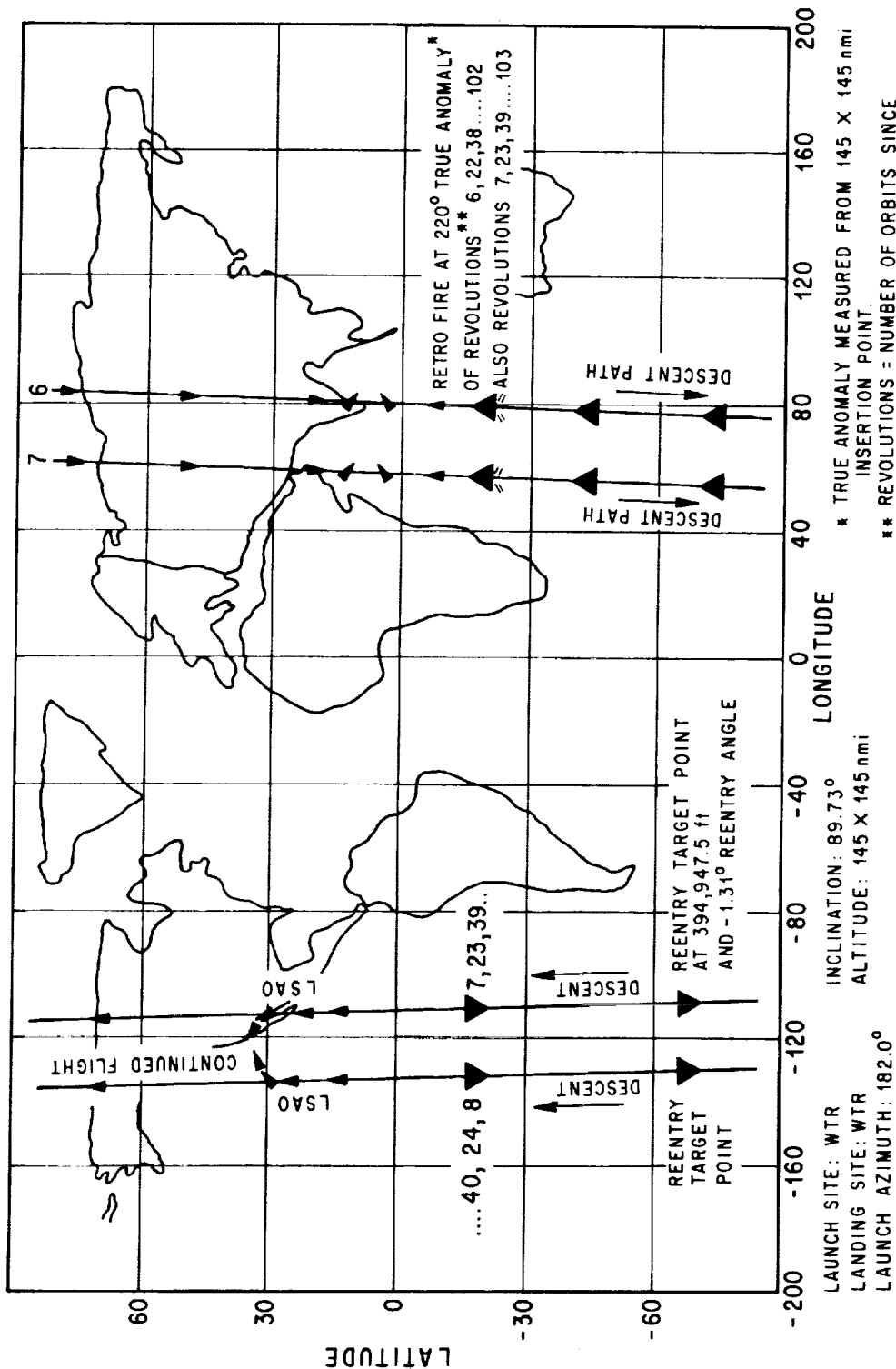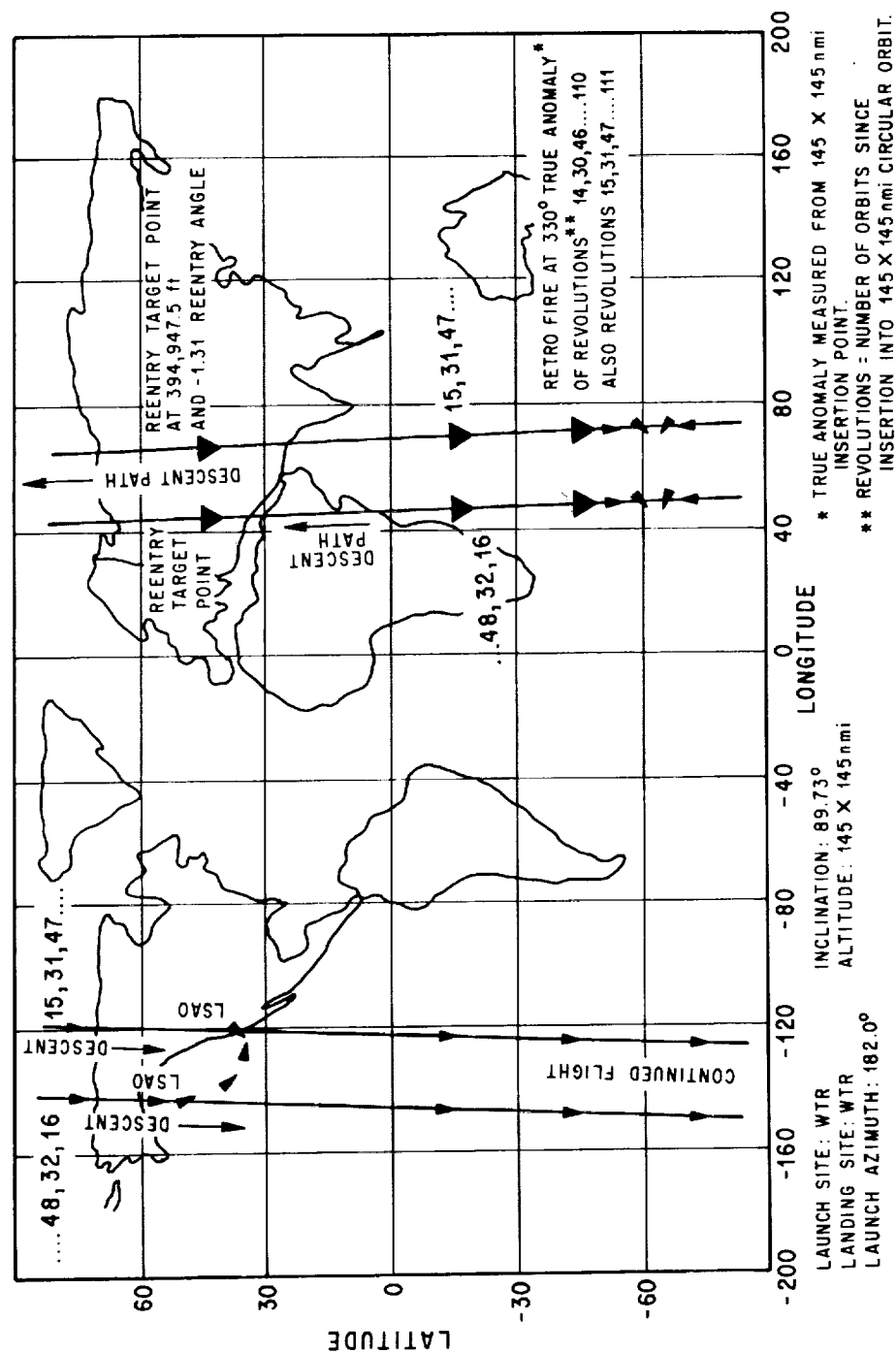
51

TABLE 2. TYPICAL SPACE SHUTTLE MISSION TWO (ADVANCED HEAO DELIVERY)

SEQUENCE OF FLIGHT EVENTS

Event	Time[a] of Initiation (Sec)	Δ Time to Next Event (Sec)	Propulsion System	Event ΔV, m/s (fps)	Resultant ha/hp km (n. mi.)	Position Latitude (deg)	Position Longitude (deg)	Position Altitude km (n. mi.)
Insertion into initial orbit of 50 by 100 n. mi.	0.0	2617.9	NA	NA	185.2 by 92.6 (100 by 50)	27.57	-66.71	92.6 (50)
First impulsive burn	2617.9	2643.2	OMS	27.58 (90.5)	185.2 by 185.2 (100 by 100)	-27.74	102.47	185.2 (100)
Second impulsive burn	5261.1	2702.1	OMS	54.02 (177.2)	370.4 by 185.2 (200 by 100)	27.70	-88.37	185.2 (100)
Third impulsive burn	7963.2	0.0	OMS	53.64 (176.01)	370.4 by 370.4 (200 by 200)	-27.66	80.59	370.4 (200)
Note:	The following events will be landing site acquisition opposite (LSAO) requiring a constant 333.89 ft/sec ΔV to achieve a reentry angle of -1.35 at 120.38 km or 394 947.5 ft. Also, the following cross-range — down-range constraints will be met when the spacecraft is at 120.38 km. (1) 0 < cross-range < 1100 n. mi. (2) 4475 < down-range < 6475 n. mi.							
LSAO 1st revolution deorbit	7963.2	5971.3	OMS	101.77 (333.89)	370.4 by 0.0 (200 by 0)	-27.66 / 17.34	80.59 / -176.78	370.4 / 120.38
LSAO 2nd revolution deorbit	13934.5	52823.6	OMS	101.77 (333.89)	370.4 by 0.0 (200 by 0)	-20.02 / 26.53	87.89 / -170.48	370.4 / 120.38
LSAO 11th revolution deorbit	66758.1	5971.4	OMS	101.77 (333.89)	370.4 by 0.0 (200 by 0)	4.13 / -27.27	77.29 / -174.2	370.4 / 120.38
LSAO 12th revolution deorbit	72729.5	5971.4	OMS	101.77 (333.89)	370.4 by 0.0 (200 by 0)	-10.34 / -19.02	79.15 / -167.33	370.4 / 120.38
LSAO 13th revolution deorbit	78700.9	5971.4	OMS	101.77 (333.89)	370.4 by 0.0 (200 by 0)	-22.37 / -5.85	83.37 / -164.24	370.4 / 120.38
LSAO 14th revolution deorbit	84672.2	5512.0	OMS	101.77 (333.89)	370.4 by 0.0 (200 by 0)	-28.31 / 8.66	91.49 / -162.50	370.4 / 120.38
LSAO 15th revolution deorbit	90184.2	5971.4	OMS	101.77 (333.89)	370.4 by 0.0 (200 by 0)	-28.35 / 9.00	68.85 / 174.68	370.4 / 120.38
LSAO 17th revolution deorbit	96155.6	5971.4	OMS	101.77 (333.89)	370.4 by 0.0 (200 by 0)	-25.55 / 21.64	77.94 / 179.24	370.4 / 120.38
LSAO 18th revolution deorbit	102127.0	52823.6	OMS	101.77 (333.89)	370.4 by 0.0 (200 by 0)	-15.43 / 28.14	83.66 / -172.95	370.4 / 120.38
LSAO 27th revolution deorbit	154950.6	5971.4	OMS	101.77 (333.89)	370.4 by 0.0 (200 by 0)	-1.55 / -24.88	72.00 / -176.98	370.4 / 120.38

TABLE 2. (Concluded)

SEQUENCE OF FLIGHT EVENTS

Event	Time[a] of Initiation (Sec)	Δ Time to Next Event (Sec)	Propulsion System	Event ΔV, m/s (fps)	Resultant h_a/h_p km (n. mi.)	Position Latitude (deg)	Position Longitude (deg)	Position Altitude km (n mi)
Note: From the last entry (LSAO 27th rev. deorbit), observe that there is approximately 9 revolutions per day that the landing site cannot be acquired because of vehicle cross-range constraint 1100 n. mi. Entries into the table will now be spaced to include the beginning and ending of the series of revolution meeting constraints[b]								
LSAO 33rd revolution end of series deorbit	184 348.1	58 795.0	OMS	101.77 (338.89)	370.4 by 0.0 (200 by 0)	-22.32	74.72	370.4
						25.06	175.91	120.38
LSAO 43rd revolution begin series deorbit	243 143.1	29 897.4	OMS	101.77 (338.89)	370.4 by 0.0 (200 by 0)	-7.19	66.76	370.4
						-21.41	179.64	120.38
LSAO 49th revolution end of series deorbit	272 540.5	52 823.6	OMS	101.77 (338.89)	370.4 by 0.0 (200 by 0)	-18.16	70.86	370.4
						27.38	173.17	120.38
LSAO 58th revolution begin series deorbit	325 364.1	35 368.9	OMS	101.77 (338.89)	370.4 by 0.0 (200 by 0)	1.73	59.74	370.4
						-26.40	169.42	120.38
LSAO 65th revolution end of series deorbit	360 733.0	52 823.6	OMS	101.77 (338.89)	370.4 by 0.0 (200 by 0)	-13.31	66.40	370.4
						28.44	170.84	120.38
LSAO 74th revolution begin series deorbit	413 556.6	29 397.4	OMS	101.77 (338.89)	370.4 by 0.0 (200 by 0)	-3.95	54.44	370.4
						-23.52	166.41	120.38
LSAO 79th revolution end of series deorbit	442 954.1	58 795.0	OMS	101.77 (338.89)	370.4 by 0.0 (200 by 0)	-20.66	57.85	370.4
						26.04	158.62	120.38
LSAO 90th revolution begin series deorbit	501 749.1	29 397.4	OMS	101.77 (338.89)	370.4 by 0.0 (200 by 0)	-9.5	49.29	370.4
						-19.65	162.77	120.38
LSAO 95th revolution end of series deorbit	531 146.5	52 823.7	OMS	101.77 (338.89)	370.4 by 0.0 (200 by 0)	-16.18	53.72	370.4
						27.92	156.06	120.38
LSAO 105th revolution begin final series deorbit	583 970.2	17 454.7	OMS	101.77 (338.89)	370.4 by 0.0 (200 by 0)	-0.67	42.18	370.4
						-25.30	152.97	120.38
LSAO 108th revolution final for 7-day mission deorbit	601 424.9	1 734.5	OMS	101.77 (338.89)	370.4 by 0.0 (200 by 0)	-25.34	27.29	370.4 (200)
Vehicle at 120.38 km reentry angle -1.35 and all constraints met	603 159.4	TBD	NA	NA	NA	-0.65	137.94	120.38 (65)
Landing	TBD	NA	NA	NA	NA	28.5	-80.6	0.0

a. time = elapsed seconds since insertion into 50 by 100 n. mi. orbit
b. revolution = number of orbits since insertion into 200 by 200 n. mi. circular orbit

Notes: (1) altitude: 370.4 km (200 n. mi.)
(2) time of launch: TBD
(3) inclination: 28.5
(4) launch site: ETR
(5) launch azimuth: 90 deg
(6) orbit selection: orbit altitude may vary upward as a function of changing orbit decay parameters with respect to launch date. Trapped radiation belts may cause some concern.
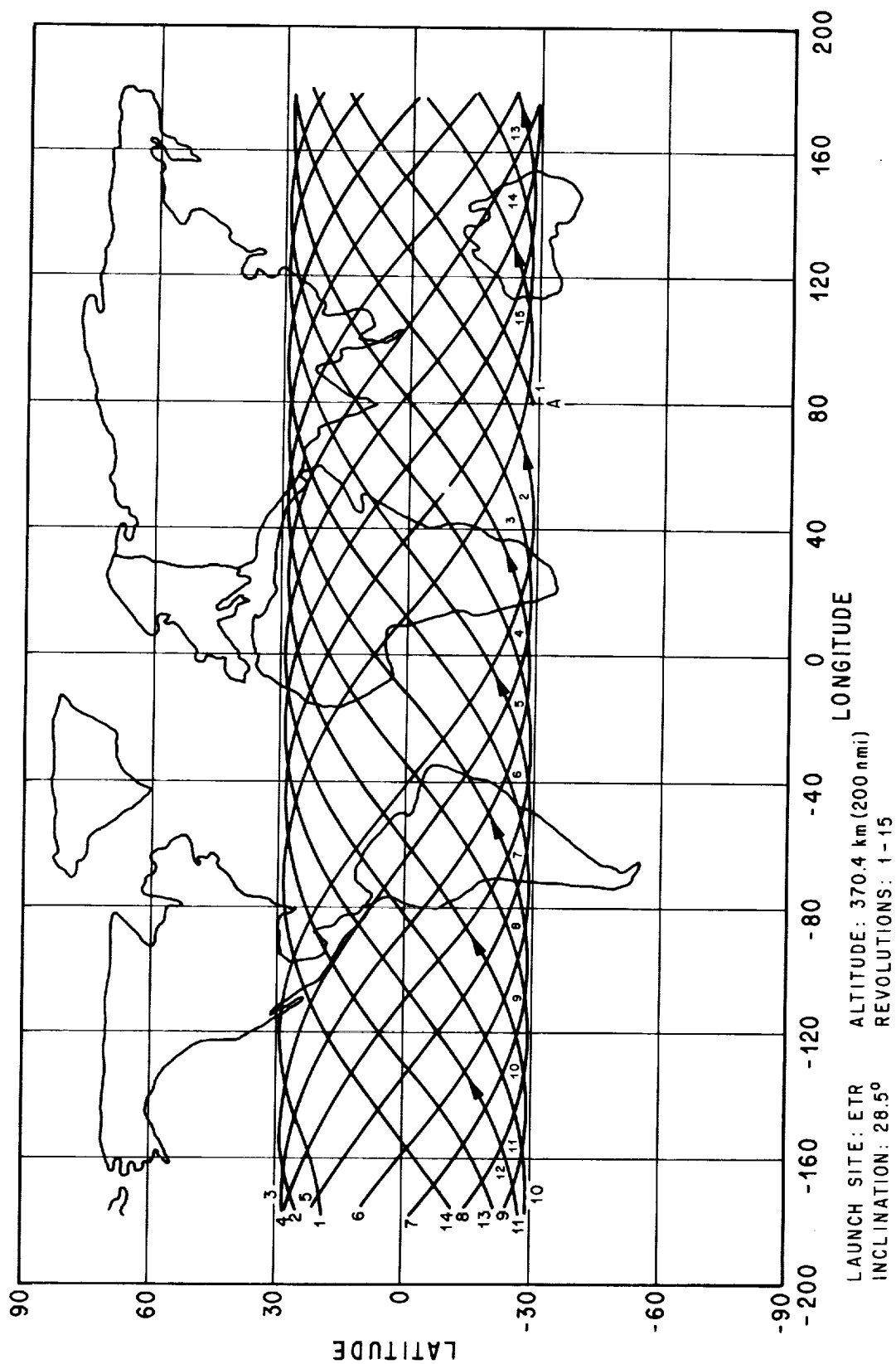
Figure 17. Typical Space Shuttle Mission Two revolutions 1-15.

LAUNCH SITE: ETR   ALTITUDE: 370.4 km (200 nmi)
INCLINATION: 28.5°   REVOLUTIONS: 1-15

54

TABLE 3. TYPICAL SPACE SHUTTLE MISSION THREE (PLACE COMM/NAV SATELLITE INTO GEOSYNCHRONOUS ORBIT — 28.5 DEG INCLINATION)

SEQUENCE OF FLIGHT EVENTS

Event	Time[a] of Initiation (Sec)	Δ Time[c] to Next Event (Sec)	Propulsion System	Event ΔV, m/s (fps)	Resultant ha hp km (n mi)	Latitude (deg)	Position Longitude (deg)	Altitude km (n mi)
Insertion into initial orbit of 50 by 100 n. mi.	0.0	2617.9	NA	NA	185.2 by 92.6 (100 by 50)	27.57	-66.71	92.6 (50)
First impulse burn	2617.0	2643.2	OMS	27.58 (90.5)	185.2 by 185.2 (100 by 100)	-27.74	102.47	185.2 (100)
Second impulsive burn	5261.1	2702.1	OMS	54.02 (177.2)	370.4 by 185.2 (200 by 100)	27.70	-88.37	185.2 (100)
Third impulsive burn	7963.2	2758.6[c] 8275.9 13793.2 19310.5	OMS	53.64 (176.01)	370.4 by 370.4 (200 by 200)	-27.66	80.59	370.4 (200)
Option no. 1[c] fire kick-stage achieve position no. 1-(Fig.18)	10721.8	43082.04	kick-stage or tug	2405.7 (7892.9)	35786.0 by 370.4 (19322 by 200)	27.61	-110.73	370.4 (200)
Option no. 1, fire kick-stage to circularize in geosync. pos. 1	53803.8	NA	kick-stage or tug	1459.5 (4788.5)	35786.1 by 35786.1	-27.79	-111.48	35786.1 (19322.9)
Option no. 2[c] fire kick-stage achieve position no. 2- (Fig. 18)	16239.1	43082.04	kick-stage or tug	2405.7 (7892.9)	35786.0 by 370.4 (19322 by 200)	27.51	-133.38	370.4 (200)
Option no. 2 fire kick-stage to circularize pos. no. 2	59321.1	NA	kick-stage or tug	1459.5 (4788.5)	35786.1 by 35786.1	-27.79	-134.53	35876.1 (19322.9)
Option no. 3[c] fire kick-stage achieve position no. 3- (Fig. 18)	21756.4	43082.04	kick-stage or tug	2405.7 (7892.9)	35786.0 by 370.4 (19322 by 200)	27.41	-156.04	370.4 (200)
Option no. 3 fire kick-stage to circularize in geosync. pos. no. 3	64838.4	NA	kick-stage or tug	1459.5 (4788.5)	35786.1 by 35786.1	-27.79	-157.58	35786.1 (19322.9)
Observe:	The time for kick-stage firing to achieve relative positions 1-15 shown in Figure 41 is sequenced exactly one revolution apart.							
Note:	All landing site acquisition opportunities for mission aborts and mission complete are the same as defined for typical Space Shuttle Mission Two.							
LSAO 108th rev.[b] final for 7-day Shuttle Mission - deorbit	601424.9	1734.5	OMS	101.77 (338.89)	370.4 by 0.0 (200 by 0)	-25.34	27.29	370.4 (200)
Vehicle at 120.38 km-reentry angle -1.35 and all other constraints met	603159.4	TBD	NA	NA	370.4 by 0.0 (200 by 0)	-0.65	137.94	120.38 (65)
Landing	TBD	NA	NA	NA	NA	28.5	-80.6	0.0

a. time = elapsed seconds since insertion into 50 by 100 n. mi. orbit
b. revolution = number of orbits since insertion into 200 by 200 n. mi. circular orbit
c. Δ time = time increment to use for firing of kick-stage or tug as a function of desired geosynchronous position

Notes: (1) altitude: Shuttle - 370.4 km (200 n. mi.) - COMM/NAV - 35786.1 km (1932.29) n. mi.
    (2) time of launch: TBD
    (3) inclination: 28.5 deg
    (4) launch site - landing site: ETR
    (5) launch azimuth: 90 deg

    (6) expendable or retrievable delta kick-stage or tug
    (7) orbit selection: the 200 n. mi. Shuttle orbit may be lowered depending on final payload weight and propellant requirements. COMM/NAV is placed in a geosynchronous orbit with the option of selecting the hovering point over a 360 deg longitudinal shift as shown in Figure 18.

55

Figure 18 illustrates the relative positioning achieved by the COMM/NAV payload as a result of firing the kickstage at increments of one revolution (5517.29 sec) of the Space Shuttle Orbiter operating in a 200 n. mi. circular orbit.

As will be explained in detail later, Figure 18 also shows the relative time averaged magnetically trapped electron particle count greater than 0.5 MeV at the different position in a geosynchronous orbit.

4. Example Rendezvous and Payload Retrieval Mission Four. For Mission Four the Space Shuttle Mission Analysis Code performs a version of the proposed USSR-SOYUZ/USA-Apollo Rendezvous and Docking Test Mission to demonstrate the Code's capability to perform rendezvous analysis involving two vehicles launched at different times and possibly from different launch sites. The simulated mission as performed is similar to the joint project Technical Proposal [13] only in the fact that an effort is made to insure that major events occur at similar times and over similar points on the surface of the earth.

Emphasis is also placed on minimizing the total Reaction Control System ΔV requirement for the Apollo pursuit vehicle in accomplishing the mission.

A current set of proposed orbit parameters were used to generate starting state vectors for both the Apollo and Soyuz vehicles. The Apollo launch site is KSC, Florida (ETR) and the Soyuz launch site is Baikonur, Kazakhstan, USSR. Other orbit parameters for each vehicle are detailed in the following tables and figures.

Table 4 shows a detailed sequence of flight events for the Apollo/Soyuz Rendezvous and Docking Test Mission including relative phase angles and Δ node angle for the two orbits. Many of the detailed onorbit operations are omitted, but again, time is allowed for the operations and is shown as "vehicle phasing".

Figure 19 illustrates the six-impulse rendezvous maneuver sequence as used in the Space Shuttle Mission Analysis Code.

Figure 20 shows the relative positions and revolutions of the Soyuz and Apollo vehicles at Apollo lift-off from KSC, Florida and the relative positions of the spacecrafts at the start of rendezvous phasing.

56

SHUTTLE ORBIT PARAMETERS AND LAUNCH SITE SAME AS FOR MISSION II i.e. ALTITUDE = 200 nmi, INCLINATION = 28.5°
MISSION REQUIRES EXPENDABLE OR RETRIEVABLE KICK-STAGE OR TUG TO PLACE COMM/NAV SATELLITE INTO A
GEOSYNCHRONOUS ORBIT 35786.1 km (19322.9 nmi) ACHIEVING INDICATED POSITIONS AS A FUNCTION OF TIME INTO THE
MISSION THAT KICK-STAGE IS ACTIVATED.
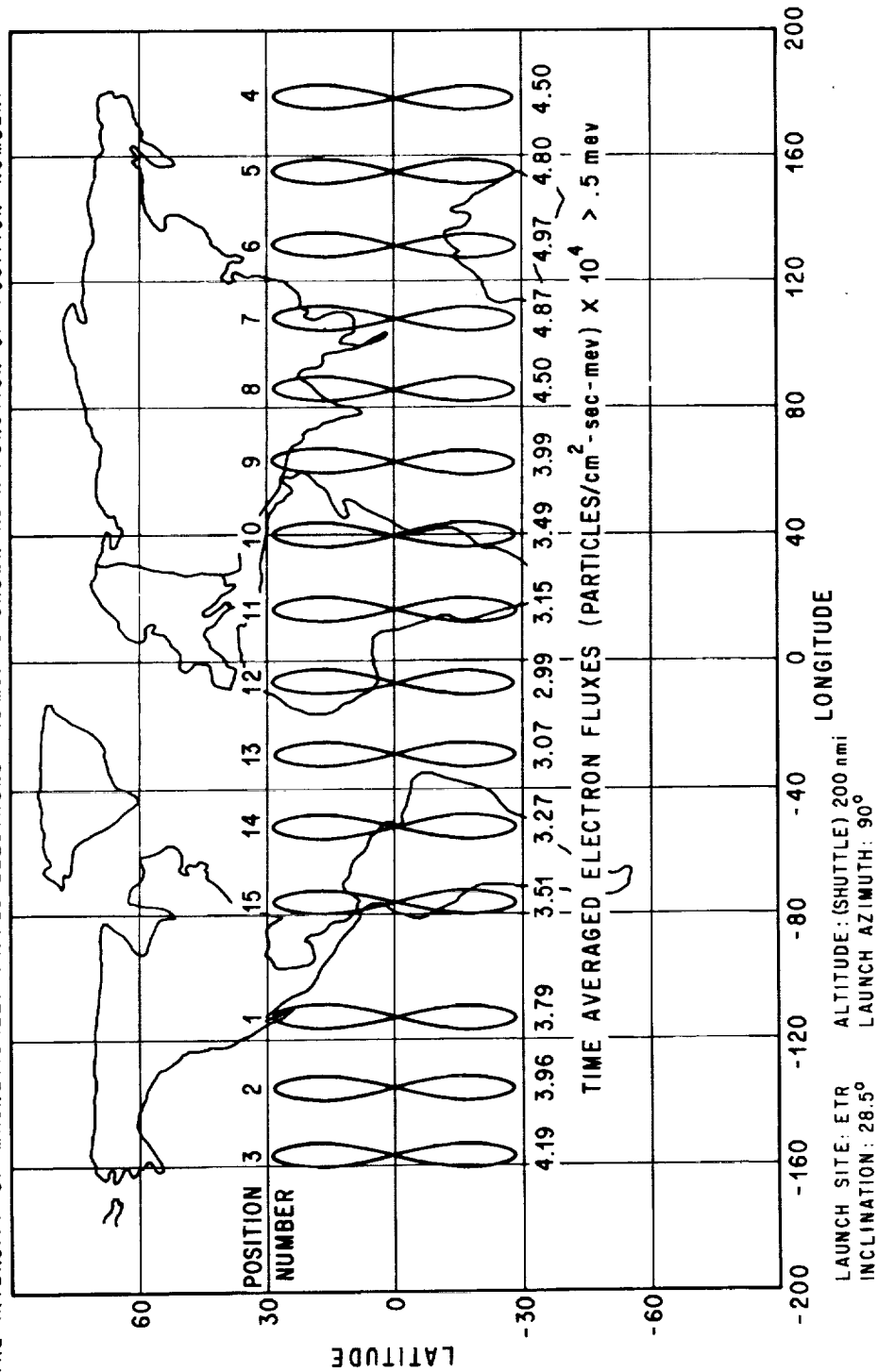THE INTENSITY OF MAGNETICALLY TAPPED ELECTRONS >.5 mev IS SHOWN AS A FUNCTION OF POSITION NUMBER.

Figure 18. Typical Space Shuttle Mission Three.

LAUNCH SITE: ETR   ALTITUDE: (SHUTTLE) 200 nmi
INCLINATION: 28.5°   LAUNCH AZIMUTH: 90°

TIME AVERAGED ELECTRON FLUXES (PARTICLES/cm^2-sec-mev) X 10^4 > .5 mev

POSITION NUMBER

LONGITUDE

LATITUDE

TABLE 4. USSR–SOYUZ/USA–APOLLO RENDEZVOUS TEST MISSION

SEQUENCE OF FLIGHT EVENTS

Event	Time[a] of Initiation Hr (Sec)	Δ Time to Next Event Hr (Sec)	Propulsion System	Event ΔV, m/s (fps)	Resultant ha/hp km (n mi)	Latitude (Deg)	Longitude (Deg)	Altitude km (n mi)	Phase Angle (Deg)	Δ Node Angle (Deg)
Soyuz lift–off	0.0 (0.0)	0.161 (580.0)	NA	NA	NA	45.38	63.16	0.0	NA	NA
Soyuz insertion 101 by 123 n. mi.	0.161 (580.0)	0.738 (2659.02)	NA	NA	227.8 by 187.1 (123.0 by 101.0)	51.41	88.88	187.1 (101)	NA	NA
Soyuz circularization 123 by 123 n. mi.	0.899 (3239.0)	6.473 (23303.6)	NA	12.02 (39.44)	227.8 by 227.8 (123.0 by 123.0)	-51.43	-102.24	227.8 (123)	NA	NA
Apollo lift–off Soyuz position	7.37 (26542.6)	0.166 (600.0)	SATURN IB	NA	0.0 by 0.0 227.0 by 227.0	28.50 27.58	-80.56 -78.41	0.0 227.8	NA	NA
Apollo insertion Soyuz position	7.54 (27142.60)	0.731 (2634.3)	NA	NA	183.3 by 149.9 227.0 by 227.0	39.29 49.78	-65.08 -36.34	149.9 227.8	22.82	0.0016
Apollo impulsive burn 99 by 113 n. mi.	8.27 (29776.9)	0.736 (2652.2)	SPS	17.61 (57.77)	209.5 by 183.3 (113.0 by 99.0)	-39.36	103.81	183.3 (99)	NA	NA
Apollo impulsive burn 113 by 113 n. mi.	9.0 (32429.1)	0.00862 (31.03)	SPS	7.66 (25.13)	209.5 by 209.5 113.0 by 113.0	39.44	-87.25	209.5 (113)	NA	NA
Apollo – phasing Soyuz – phasing	9.016 (32460.1)	1.48 (5342.73)	NA	NA	209.0 by 209.0 227.0 by 227.0	40.67 49.36	-85.15 -61.01	209.5 227.8	19.03	0.001
Apollo – phasing Soyuz – phasing	10.50 (37802.83)	1.48 (5342.73)	NA	NA	209.0 by 209.0 227.0 by 227.0	41.68 49.43	-105.88 -83.30	209.5 227.8	17.51	0.005
Apollo – phasing Soyuz – phasing	11.98 (43145.56)	1.48 (5342.73)	NA	NA	209.5 by 209.5 227.8 by 227.8	42.65 49.51	-126.54 -105.60	209.5 227.8	15.99	0.008
Apollo – phasing Soyuz – phasing	13.46 (48488.29)	1.48 (5342.73)	NA	NA	209.5 by 209.5 227.8 by 227.8	43.59 49.58	-147.15 -127.89	209.5 227.8	14.47	0.011
Apollo – phasing Soyuz – phasing	14.95 (53831.02)	1.48 (5342.73)	NA	NA	209.5 by 209.5 227.8 by 227.8	44.49 49.66	-167.68 -150.18	209.5 227.8	12.95	0.015
Apollo – phasing Soyuz – phasing	16.43 (59173.75)	1.48 (5342.73)	NA	NA	209.5 by 209.5 227.8 by 227.8	45.34 49.73	171.83 -172.47	209.5 227.8	11.44	0.018
Apollo – phasing Soyuz – phasing	17.92 (64516.48)	1.48 (5342.73)	NA	NA	209.5 by 209.5 227.8 by 227.8	46.16 49.80	151.43 165.24	209.5 227.8	9.92	0.021
Apollo – phasing Soyuz – phasing	19.40 (69859.21)	1.48 (5342.73)	NA	NA	209.5 by 209.5 227.8 by 227.8	46.93 49.87	131.08 142.95	209.5 227.8	8.40	0.025
Apollo – phasing Soyuz – phasing	20.88 (75201.94)	1.48 (5342.73)	NA	NA	209.5 by 209.5 227.8 by 227.8	47.65 49.94	110.81 120.66	209.5 227.8	6.88	0.028
Apollo – phasing Soyuz – phasing	22.37 (80544.67)	1.48 (5342.73)	NA	NA	209.5 by 209.5 227.8 by 227.8	48.32 50.00	90.60 98.38	209.5 227.8	5.36	0.031
Apollo – phasing Soyuz – phasing	23.85 (85887.40)	1.48 (5342.73)	NA	NA	209.0 by 209.0 227.0 by 227.0	48.94 50.07	70.45 76.09	209.0 227.0	3.84	0.035
Apollo – phasing Soyuz – phasing	25.34 (91230.13)	1.48 (5342.73)	NA	NA	209.0 by 209.0 227.0 by 227.0	49.50 50.14	50.36 53.81	209.0 227.0	2.32	0.038
Apollo – phasing Soyuz – phasing	26.82 (96572.8)	0.051 (186.35)	NA	NA	209.0 by 209.0 227.0 by 227.0	50.00 50.20	30.33 31.53	209.0 227.0	0.807	0.041
Apollo plane change Soyuz position	26.87 (96759.15)	0.425 (1533.05)	SPS	6.11 (20.04)	209.0 by 209.0 227.0 by 227.0	51.72 51.71	49.40 50.61	209.0 227.0	0.757	0.0
Apollo (TPI) Soyuz position	27.303 (98292.2)	0.57 (2077.7)	SPS	6.5 (21.32)	230.0 by 207.0 227.0 by 227.0	-10.80 -11.02	141.55 141.77	209.0 227.0	0.30	0.0
Apollo (TPF) Soyuz position	27.88 (100369.9)	0.194 (701.13)	SPS	6.5 (21.32)	227.0 by 227.0 227.0 by 227.0	-19.98 -19.98	-72.55 -72.55	227.0 227.0	0.004	0.0
Station keeping and flyaround	28.07 (101071.04)	0.194 (701.13)	RCS	5.2 (17.06)	227.0 by 227.0	16.70	-45.15	227.0	0.0	0.0
Apollo – Soyuz docking	28.27 (101772.1)	TBD	RCS	2.2 (7.21)	227.0 by 227.0	47.02	-3.94	227.0	0.0	0.0

Notes: (1) Soyuz launch site: Baikonor, Kazakhstan, Initial orbit: 187.1 by 227.8 km, Inclination: 51.7227 deg
    (2) Apollo launch site: Kennedy Space Flight Center, Initial orbit: 149.9 by 183.3 km, Inclination: 51.7227 deg
    (3) Apollo insertion condition: Launch azimuth: 39.38 deg; Latitude: 39.29 deg; Longitude: 65.08 deg; descending node: 155.259 deg
    (4) Apollo launch time: 7.3729 hrs after Soyuz lift–off
    (5) Apollo phasing orbit: 209.48 km circular (113 n. mi.)
    (6) Soyuz phasing orbit: 227.80 km circular (123 n. mi.)

APOLLO PHASING
ORBIT 209.5 km

SOYUZ CIRCULAR
ORBIT 227.8 km

183.3 km

$\Delta h \approx 18.5$ km
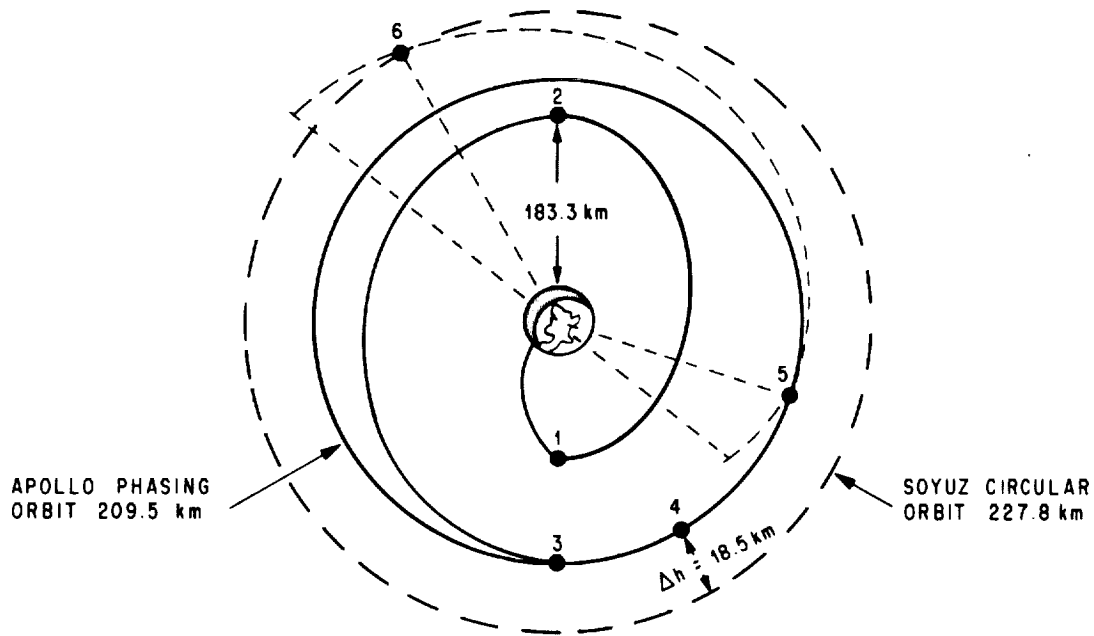
1. INSERTION - 150.0 X 183.3 km

2. IMPULSE BURN - 183.3 X 209.5 km

3. IMPULSE BURN - CIRCULARIZATION 209.5 km

4. PLANE CHANGE TO CORRECT Δ NODE ERROR

5. TERMINAL PHASE INITIATION - 207 X 230 km

6. TERMINAL PHASE FINAL - 227.8 X 227.8 km

Figure 19. Orbit geometry of Apollo's six
impulse rendezvous maneuver sequence.

Figure 21 illustrates the points above the earth where terminal phase initiation (TPI) and the final terminal phase (TPF) occur and the docking revolution which very closely approximates the time and position for these Soyuz/Apollo maneuvers as set forth in Reference 13.

USSR-SOYUZ/USA-APOLLO RENDEZVOUS TEST MISSION
APOLLO PHASING ORBIT: 209.48 km CIRCULAR (113 n mi)
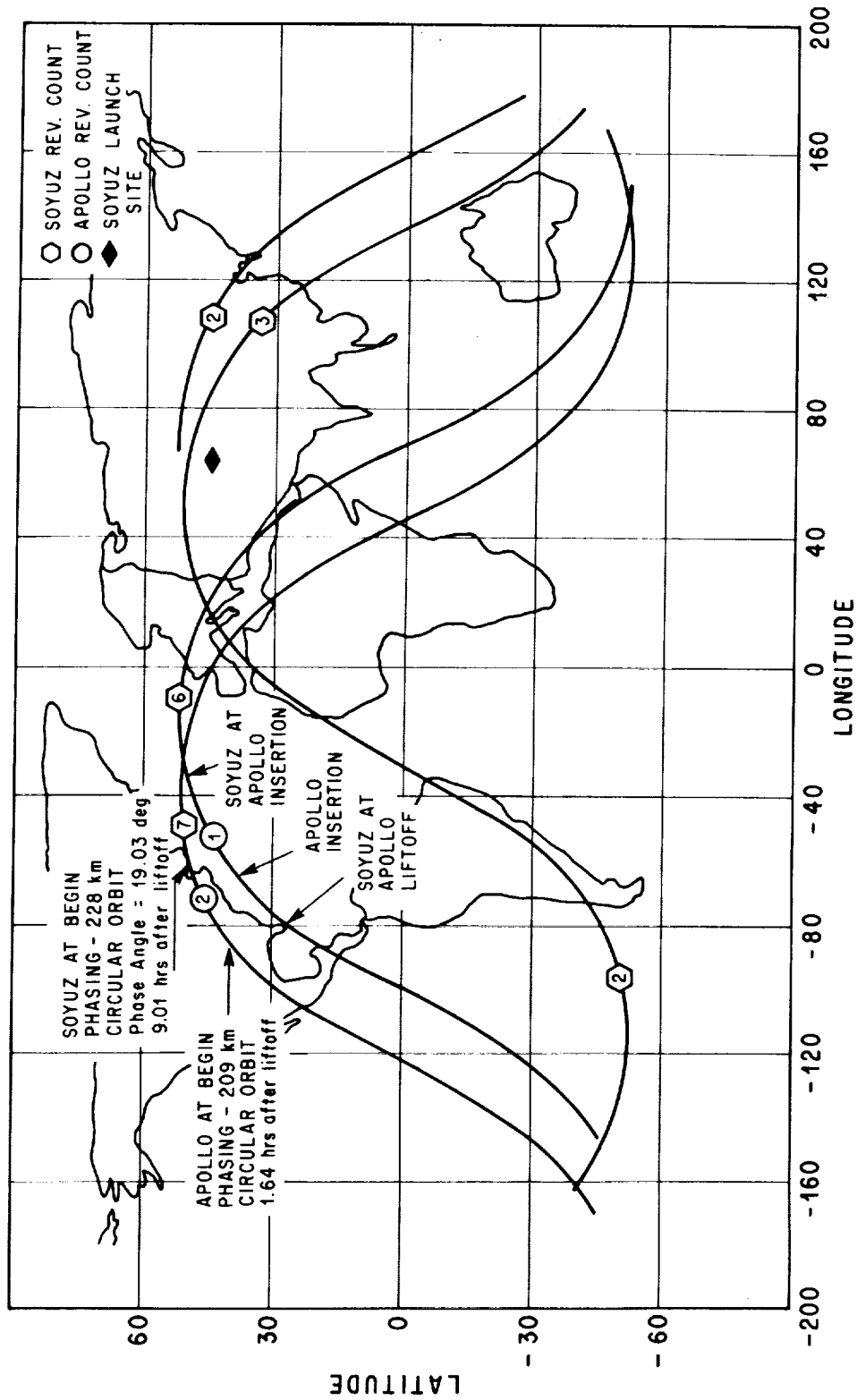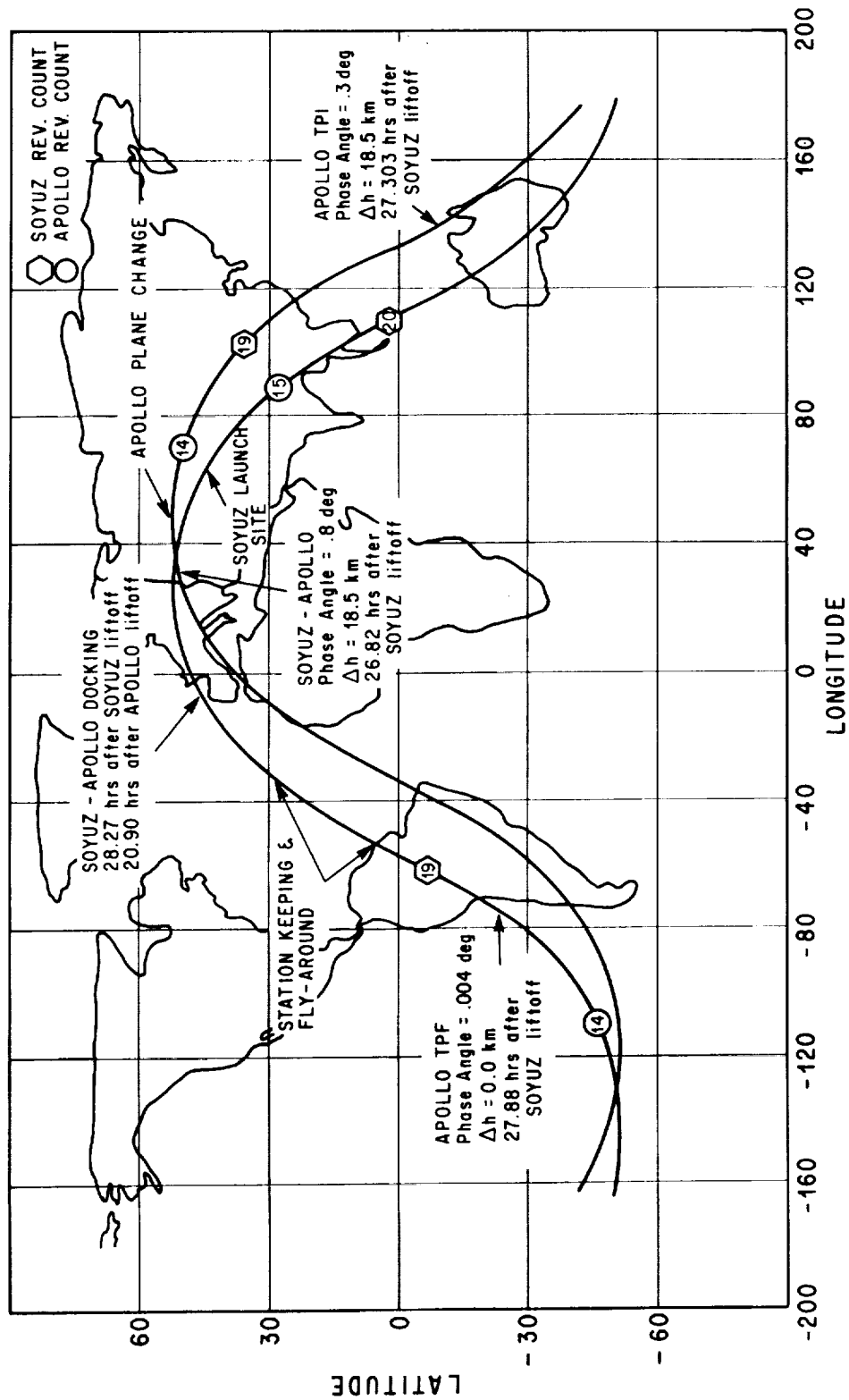SOYUZ PHASING ORBIT: 227.80 km CIRCULAR (123 n mi)

Figure 20. Apollo liftoff and begin Soyuz Apollo phasing revolutions.

60

USSR - SOYUZ / USA - APOLLO RENDEZVOUS TEST MISSION
APOLLO PHASING ORBIT: 209.48 km CIRCULAR (113 n mi)
SOYUZ PHASING ORBIT: 227.80 km CIRCULAR (123 n mi)

⬡ SOYUZ REV. COUNT
⭙ APOLLO REV. COUNT

APOLLO PLANE CHANGE

APOLLO TPI
Phase Angle = .3 deg
Δh = 18.5 km
27.303 hrs after
SOYUZ liftoff

SOYUZ LAUNCH
SITE

SOYUZ - APOLLO
Phase Angle = .8 deg
Δh = 18.5 km
26.82 hrs after
SOYUZ liftoff

SOYUZ - APOLLO DOCKING
28.27 hrs after SOYUZ liftoff
20.90 hrs after APOLLO liftoff

STATION KEEPING &
FLY - AROUND

APOLLO TPF
Phase Angle = .004 deg
Δh = 0.0 km
27.88 hrs after
SOYUZ liftoff

LONGITUDE

LATITUDE

Figure 21. Apollo terminal phase and Soyuz Apollo docking revolution.

61

C. Task 3 – Space Radiation Analysis

The computation results of Task 3 will demonstrate the capability of the Space Shuttle Mission Analysis Code to perform space radiation environment analyses of magnetically trapped electrons and protons. These analyses will define the possible radiation hazards associated with a specific mission, thus providing useful data for consideration in mission design options.

Elements of Task 3 included the integration of the codes' trajectory calculation techniques and space radiation environment models in the form of data decks provided by Dr. James I. Vette [9], et al., containing the measured omnidirectional flux of trapped electrons and protons at all defined spatial points.

Since there has been some expressed concern because of possible trapped radiation hazard associated with placing an advanced HEAO satellite in an initial orbit greater than 200 n. mi., space radiation analysis for the example Space Shuttle Mission Two was performed for altitudes of 200 n. mi. and 500 n. mi.

Time-averaged differential and integral spectrum data for this mission will be presented in subsequent figures along with comparative spectrum data associated with the two indicated altitudes, holding other orbit parameters for the mission constant. It is evident from the configurations of trapped electrons and protons in the South Atlantic anomaly that the time-averaged spectrum intensity is a function of the orbital inclination as well as altitude.

Another aspect of defining the space radiation hazard involves the use of a solar electric propulsion stage as a final tug to transport and possibly retrieve payloads for certain Space Shuttle/Tug missions.

The specific problem is then to define the number and energies of magnetically trapped protons and electrons encountered on a specific mission; converting these particles into 1 MeV-equivalent electrons and applying a tabulated solar cell damage factor to arrive at relative power loss for each mission.

This can be done by flying a simulated low-thrust trajectory through the space radiation environment model and computing the particle fluxes at all spatial points along the way. The first simulation is flown without power loss, whereas a trajectory for comparison includes a power degradation model which is linear with respect to the particle accumulation rate.

62

By knowing the environment, the damage to the solar cells and, thus, the degradation of the available power may be assessed as a function of the particular mission.

Obviously a loss of power lowers the available thrust of the stage and this fact must be taken into consideration when establishing time-lines for a particular Space Shuttle/Tug mission.

When the power loss is known as a function of time, this enables a more accurate trajectory to be calculated, using previously defined methods.

Experiments and theoretical analyses are currently underway to determine the dose rates and damage factors on specific solar cell models after being bombarded by various energy levels of protons and electrons.

Figure 22 shows the time-averaged proton flux encountered during typical Space Shuttle Mission Two (200 n. mi.) and the relative particle population at an altitude of 500 n. mi. for the same mission.

Figure 23 shows the same information for time-averaged electron fluxes for Mission Two.

Figure 24 gives the differential and integral energy spectra for protons; also the total number of particles encountered during the 7 days of Mission Two at 200 n. mi.

Figure 25 shows the same information for protons, but at an altitude of 500 n. mi., for Mission Two.

Figure 26 shows the differential and integral energy spectra for electrons and the total number of particles of all energies encountered during the 7 days of Mission Two at 200 n. mi.

Figure 27 shows the same information for electrons but at an altitude of 500 n. mi. for Mission Two.

Figure 28 shows the proton isoflux contours ($E > 50$ MeV) in the South Atlantic anomaly at an altitude of 145 n. mi.

Figure 29 shows the greatly expanded proton isoflux contours with higher intensities ($E > 50$ MeV) at an altitude of 500 n. mi. over the South Atlantic anomaly.

Figure 30 shows the electron isoflux contours for passes through the South Atlantic anomaly at an altitude of 145 n. mi.

Figure 31 shows the projected effect of the magnetically trapped space-- radiation environment on an unshielded solar electric low-thrust tug orbital transfer from a 20 000 km circular orbit to geocynchronous altitude at inclinations of 28.5 and 0.0 deg. It should be noted, that for this particular mission, a relatively thin transparent glass shield would reduce the total power loss over the mission to less than 3 percent. However, if a mission is started at a significantly lower altitude, power loss due to solar cell damage will cause increased concern to mission analysts with regard to mission duration and whether a particular mission can be flown.

Figure 32 gives an indication of the kinds of problems associated with solar electric low-thrust orbital transfers if a mission is initiated at unacceptably low altitudes. With little or no shielding, the low energy proton environment may cause accumulated power losses in excess of 50 percent over relatively short mission durations, which renders some missions impossible to be flown. However, adequate shielding of the solar cells can reduce the accumulated power loss to acceptable levels; i.e., in the 10 to 20 percent range.
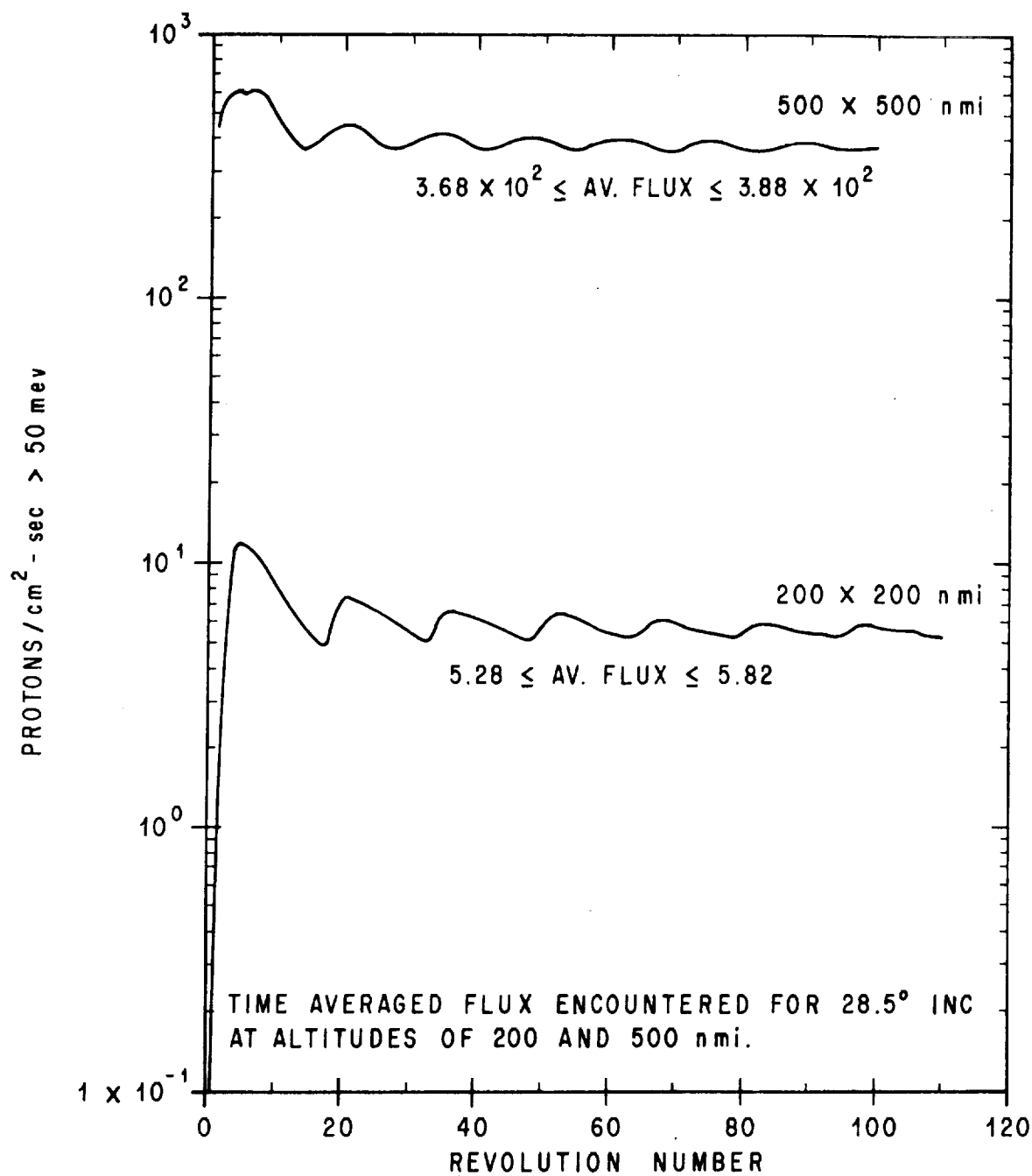
Figure 22. Typical Space Shuttle Mission Two (AHD) radiation analysis
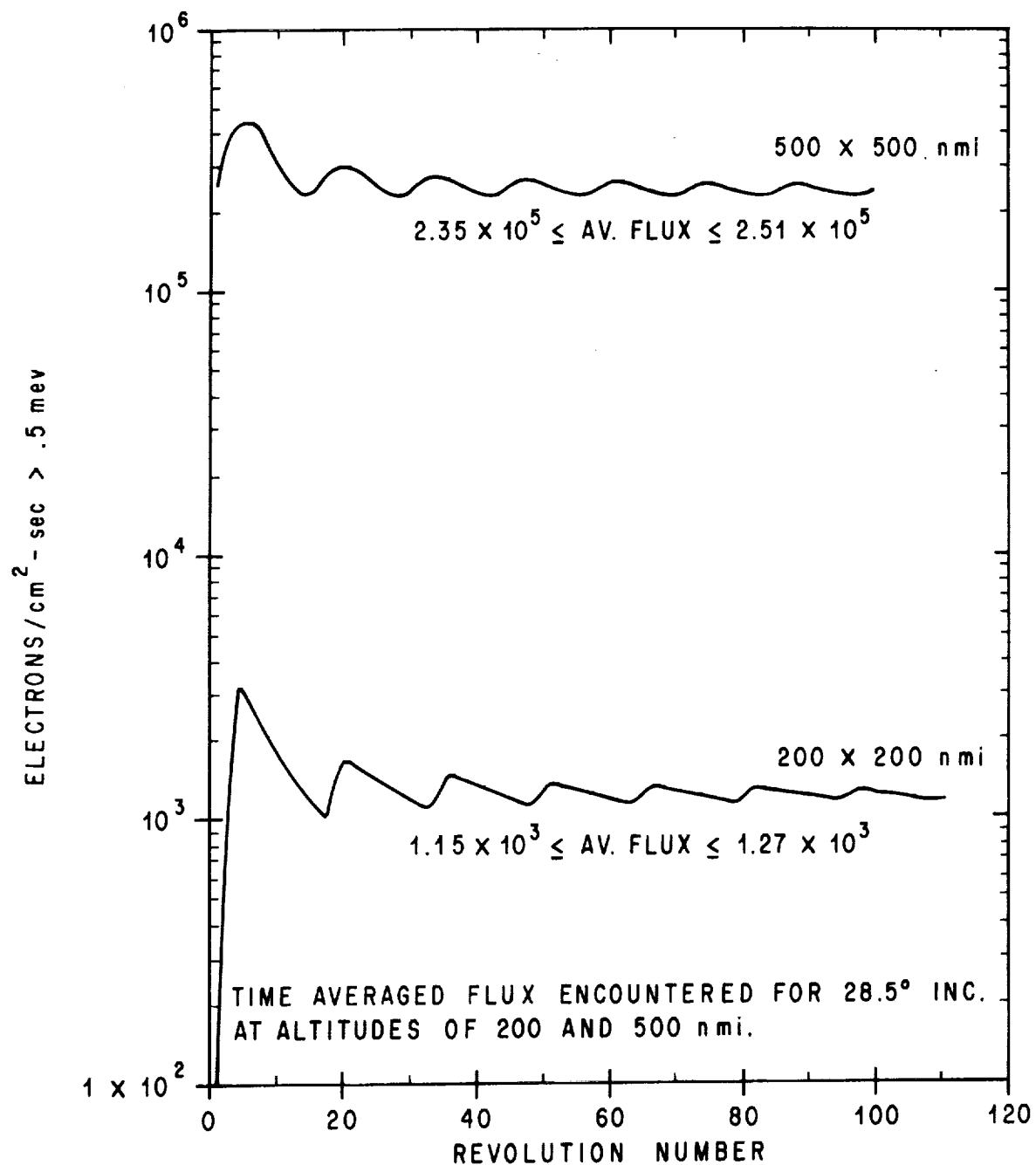(trapped protons > 50 mev).

Figure 23. Typical Space Shuttle Mission Two (AHD) radiation analysis
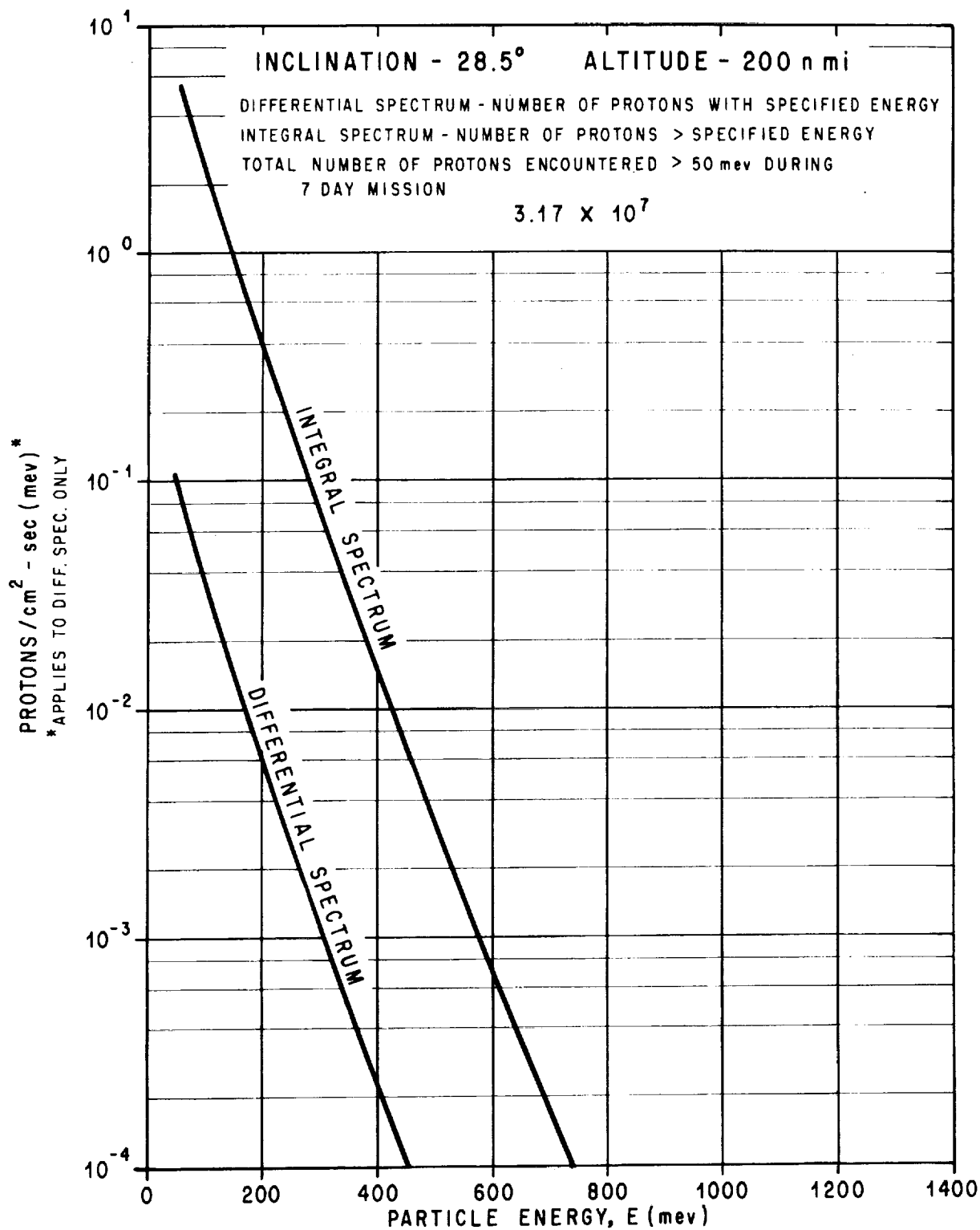(trapped electrons > 0.5 mev).

INCLINATION - 28.5°   ALTITUDE - 200 n mi

DIFFERENTIAL SPECTRUM - NUMBER OF PROTONS WITH SPECIFIED ENERGY

INTEGRAL SPECTRUM - NUMBER OF PROTONS > SPECIFIED ENERGY

TOTAL NUMBER OF PROTONS ENCOUNTERED > 50 mev DURING
7 DAY MISSION

3.17×10^{7}

INTEGRAL SPECTRUM

DIFFERENTIAL SPECTRUM

PROTONS / cm^2 - sec (mev) *
*APPLIES TO DIFF. SPEC. ONLY

PARTICLE ENERGY, E (mev)

Figure 24. Typical Space Shuttle Mission Two
time averaged energy spectra (protons).
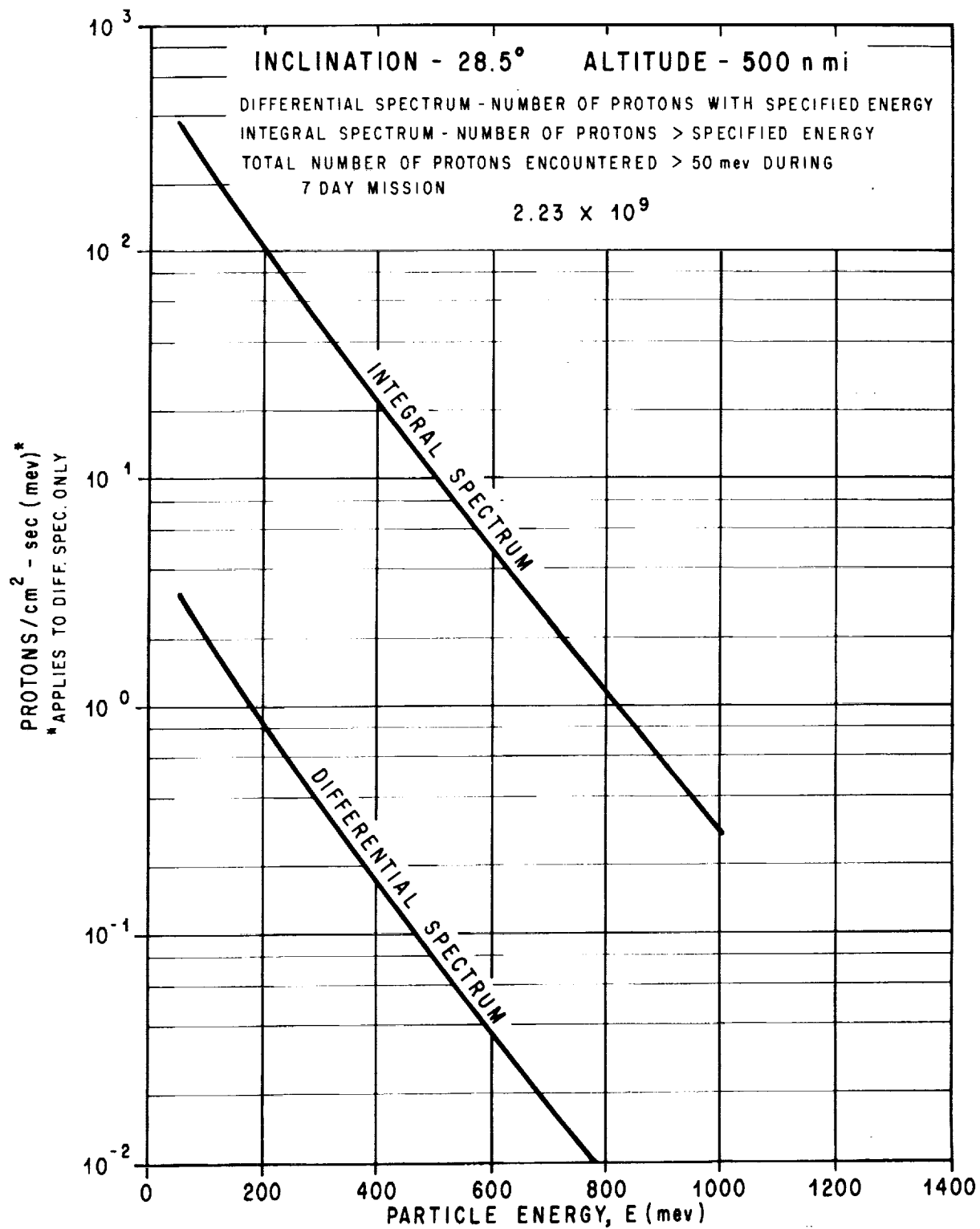
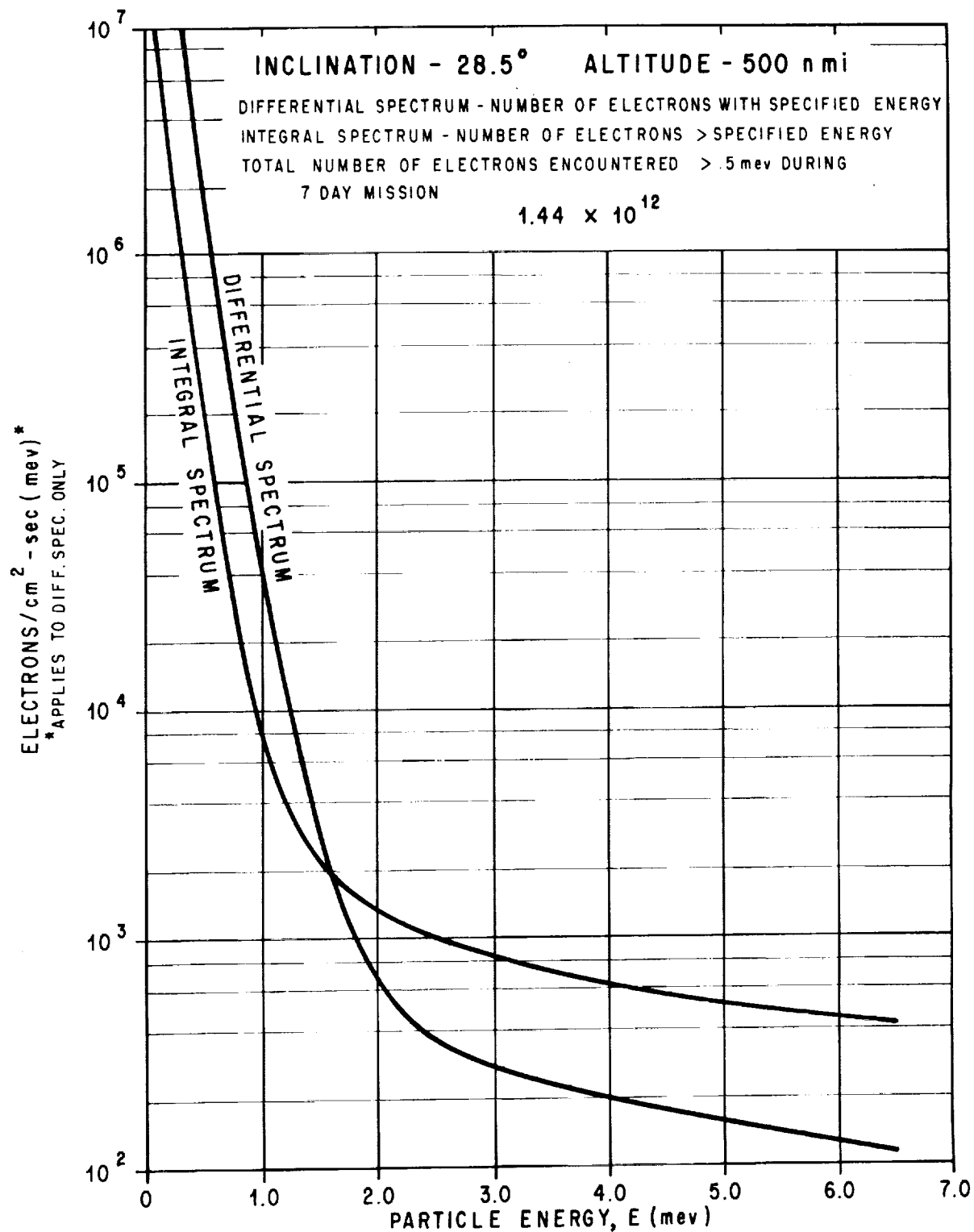Figure 25. Typical Space Shuttle Mission Two time averaged energy spectra (protons).

INCLINATION - 28.5°   ALTITUDE - 200 nmi

DIFFERENTIAL SPECTRUM - NUMBER OF ELECTRONS WITH SPECIFIED ENERGY
INTEGRAL SPECTRUM - NUMBER OF ELECTRONS > SPECIFIED ENERGY
TOTAL NUMBER OF ELECTRONS ENCOUNTERED > .5 mev DURING
7 DAY MISSION
7.02×10^9
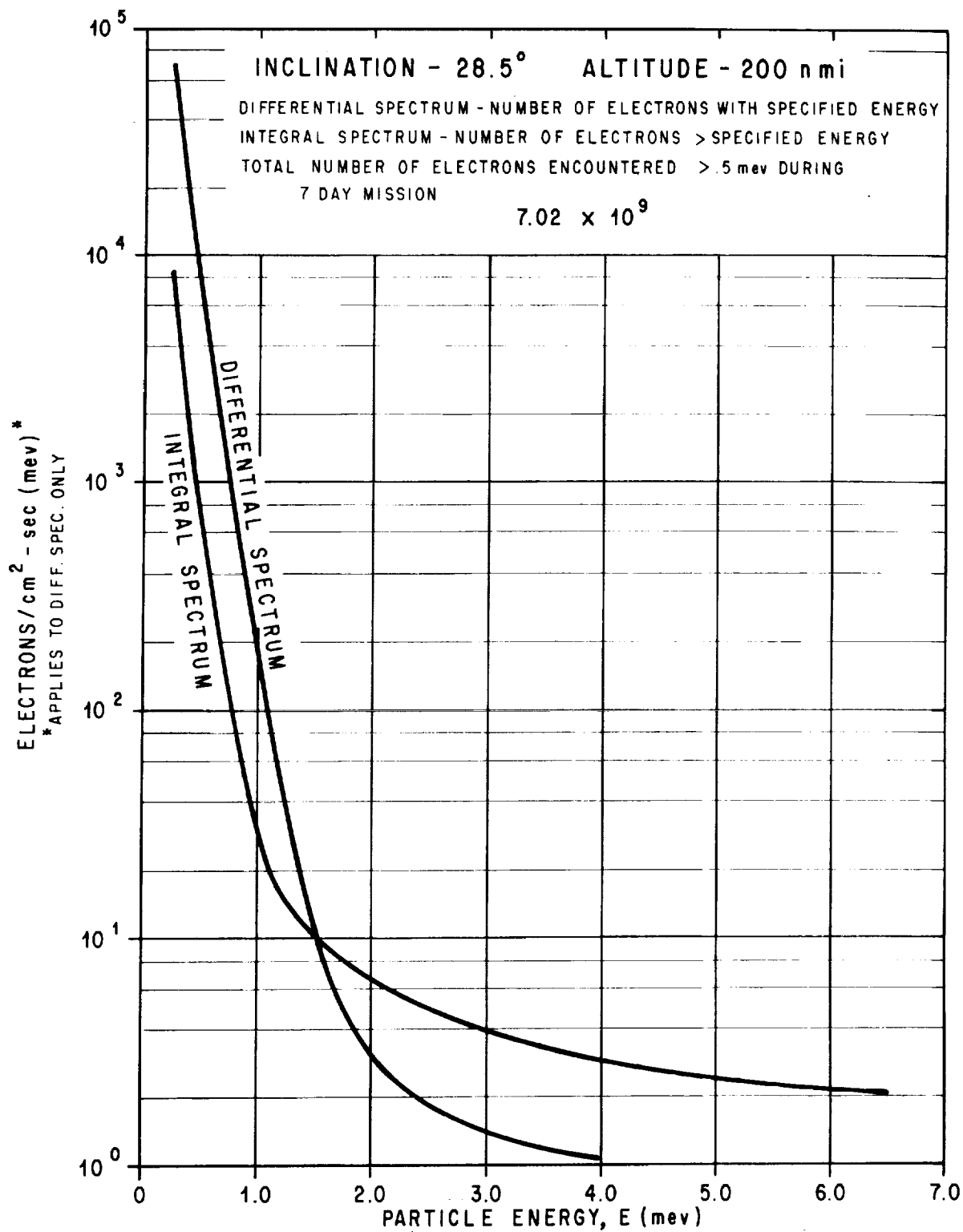
Figure 26. Typical Space Shuttle Mission Two
time averaged energy spectra (electrons).

69

Figure 27. Typical Space Shuttle Mission Two
time averaged energy spectra (electrons).

70
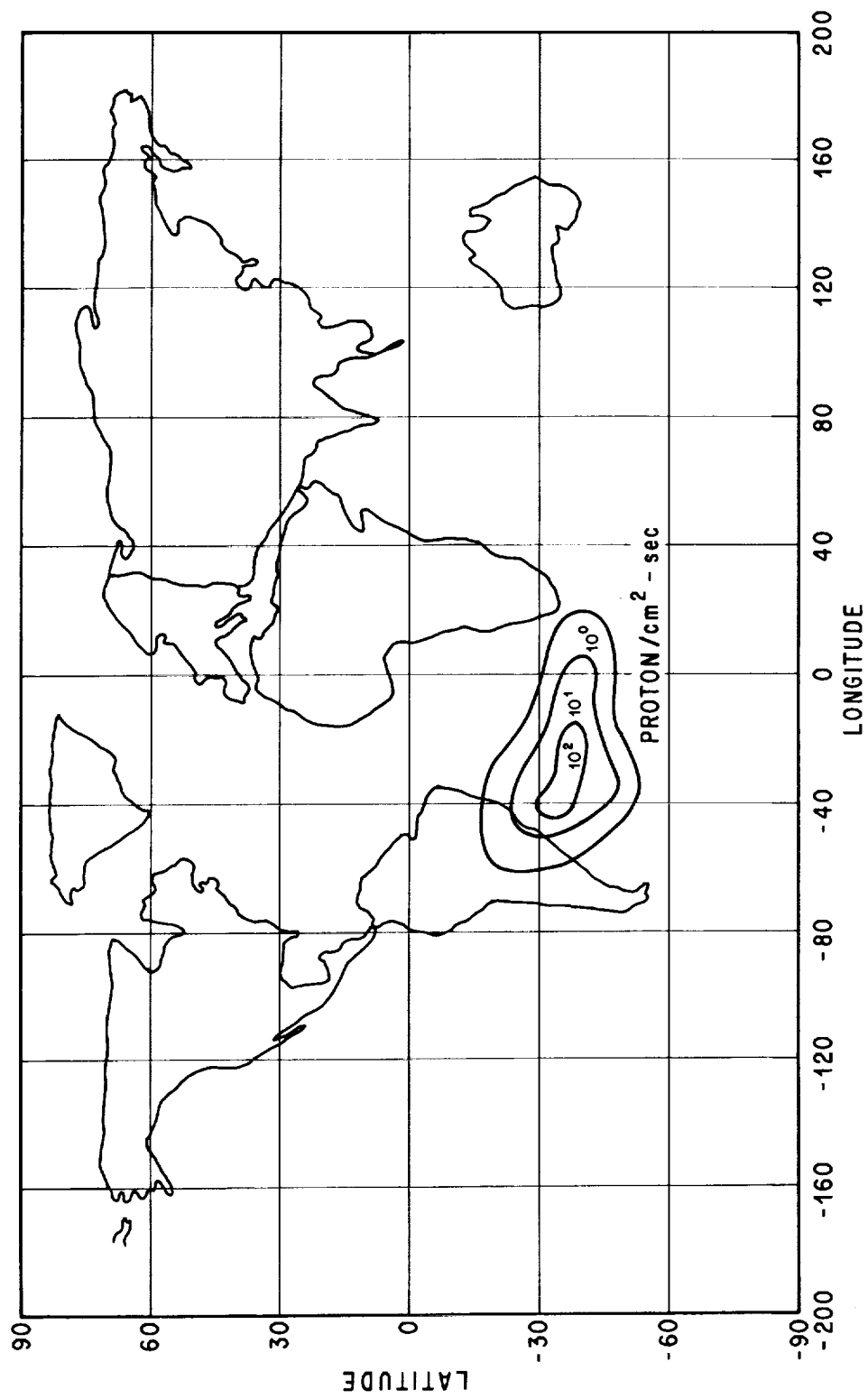
Figure 28. Proton isoflux contours at an altitude of 268.54 km (145 n. mi.) South Atlantic radiation anomaly producing total proton flux > 50 mev (AP7 data) for typical Space Shuttle Mission One (ERTSL).
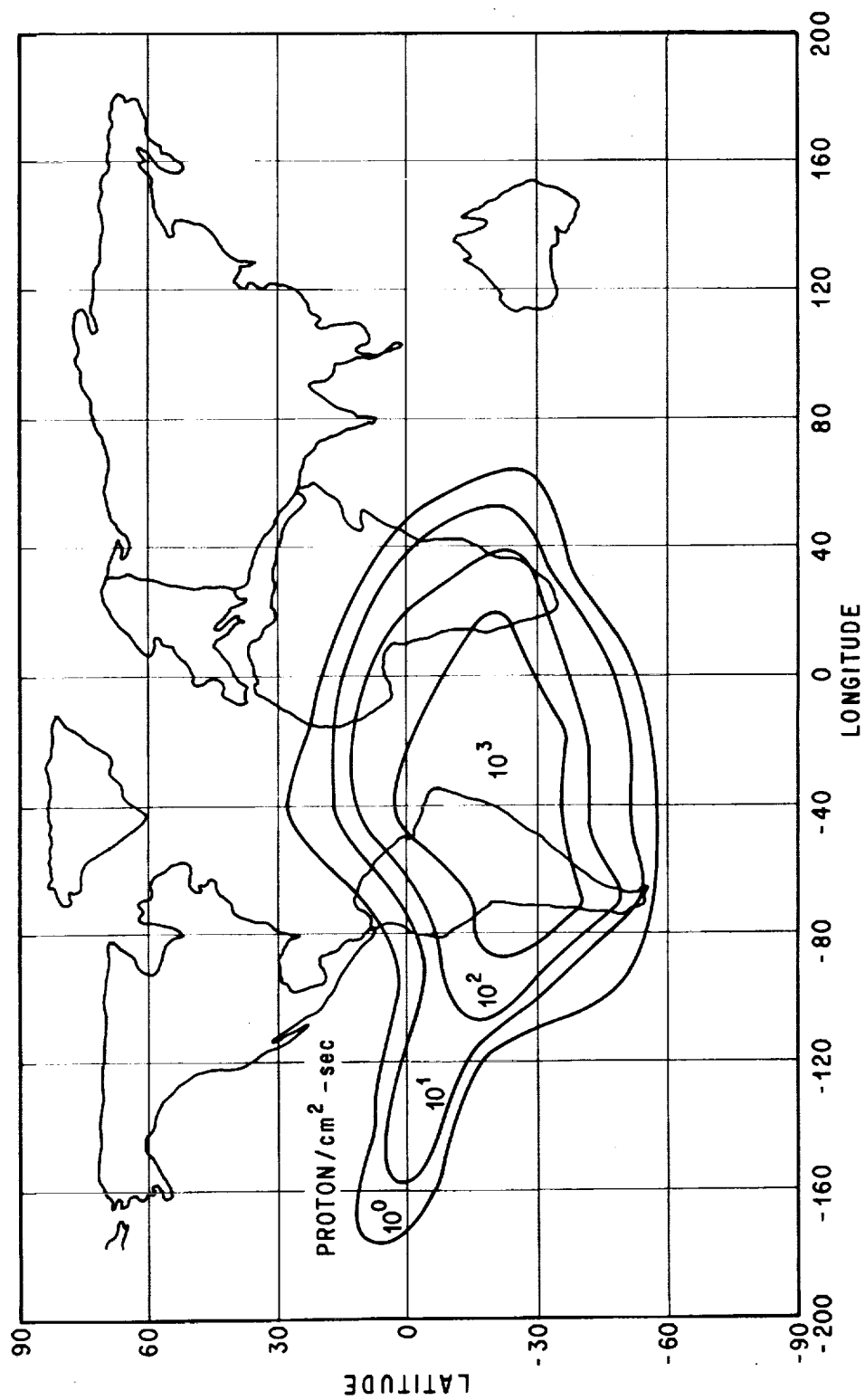
71

Figure 29. Proton isoflux contours at an altitude of 926 km (500 n. mi.) South Atlantic radiation anomaly producing total proton flux > 50 mev (AP7 data) for typical Space Shuttle Mission One (ERTSL).
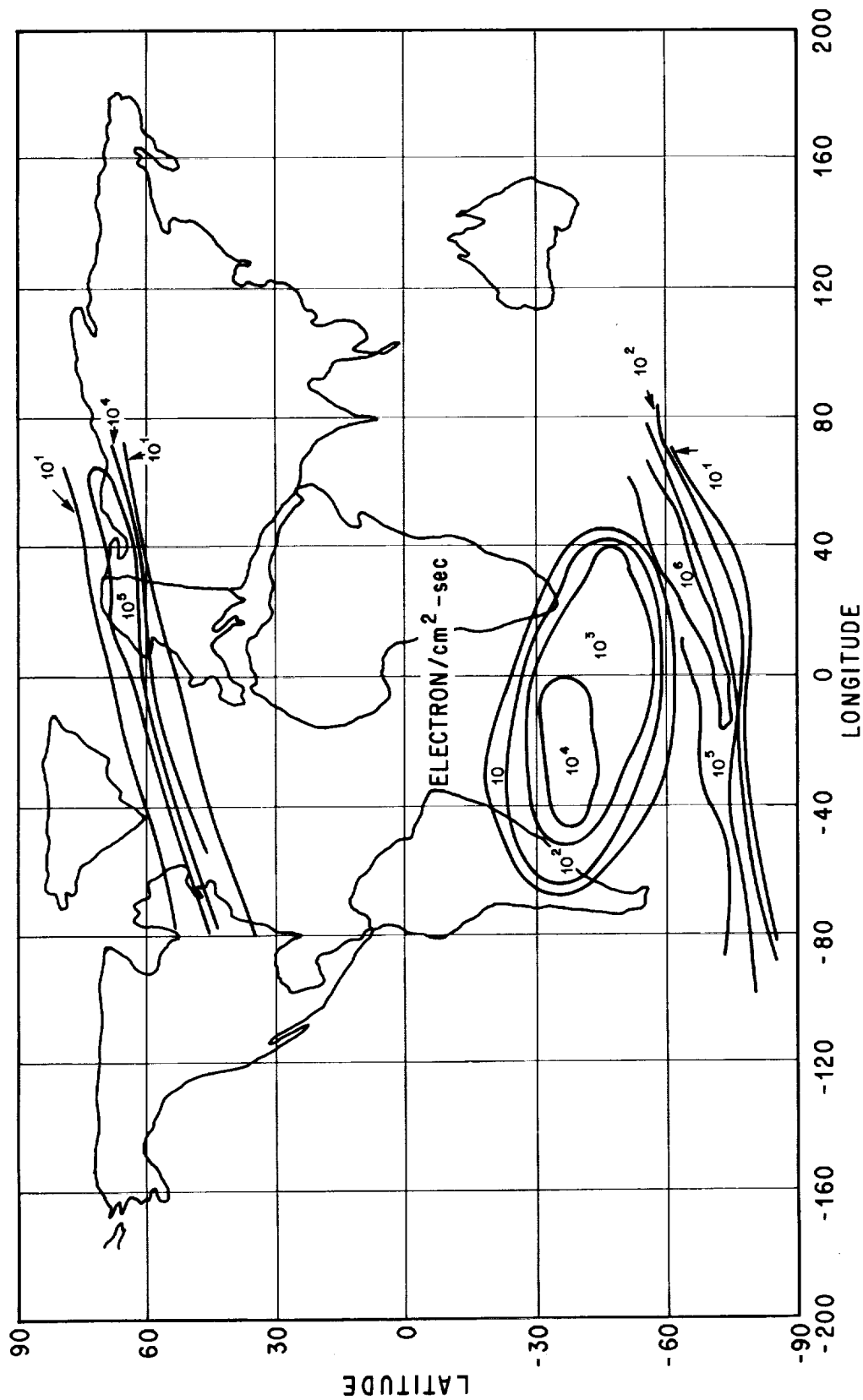
72

Figure 30. Electron isoflux contours at an altitude of 268.54 km (145 n. mi.) (1968 data, Vette) South Atlantic radiation anomaly producing partial electron flux > 0.5 mev as seen by typical Space Shuttle Mission One (ERTSL).

73

SECTION IV. CONCLUSION

It has been demonstrated that the Space Shuttle Rendezvous, Radiation and Reentry Analysis Code is a basic and versatile Space Shuttle Mission design and analysis tool which allows for extensive user interaction and flexibility through the utilization of a relatively small computer (IBM 7044). It is hoped that the foregoing presentations concerning the development and applications of the code will render insight to persons engaged in preliminary Space Shuttle mission designing, as to whether the illustrated features of the code are applicable to their specific studies and problems. The capability of the code is currently being expanded to include elliptical to circular low-thrust orbital transfers, a more sophisticated power degradation model and other effects on low-thrust trajectory analysis such as shadowing.

Mission analysis data generated by this code have been compared favorably with data generated from other sources. Source decks, listings and other specific information concerning the use of the Code are available from the author upon request.

REFERENCES

1. Nelson, W. C. and Loft, E. E.: Space Mechanics. Prentice-Hall, Inc., Englewood Cliffs, N. J., 1962.

2. Roy, A. E.: The Foundations of Astrodynamics. The Macmillan Company, New York, Collier-Macmillan Limited, London, 1965.

3. Van De Kamp, Peter: Elements of Astromechanics. W. H. Freeman and Company, San Francisco and London, 1964.

4. Constants and Related Information for Astrodynamic Calculation, 1968. JPL Technical Report 32-1306.

5. Danby, J. M. A.: Fundamentals of Celestial Mechanics. The Macmillan Company, New York, 1962.

6. McCuskey, S. W.: Introduction to Celestial Mechanics. Addison-Wesley Publishing Co. Massachusetts and London, 1963.

7. Shuttle Orbital Applications/Requirements (SOAR), Phase A Final Report Executive Summary; Phase A Final Report. Technical volume IV, System Analysis — Mission Operations, NASA-MSFC Contract NAS8-26790, performed by McDonnell Douglas and supported by Martin Marietta, TRW Inc., and IBM, 1971.

8. Elrod, Wendell and Duncan, John R.: Private Communications, NASA-MSFC, AERO-Astrodynamics Laboratory.

9. Vette, J. I., et al.: Models of the Trapped Radiation Environment. Volumes 1 and 2, NASA SP-3024, 1966.

10. McIlwain, C. E.: Coordinates for Mapping the Distribution of Magnetically Trapped Particles. J. Geophys. Res. 66:3681-4078, 1963.

11. Burrell, M. O.; Wright, J. J.; and Stern, H. E.: Private Communications, NASA-MSFC, Space Sciences Laboratory.

REFERENCES (Concluded)

12. McCormac, B. M., et al.: Radiation Trapped in the Earth's Magnetic Field. D. Reidel Publishing Company, Dordrecht-Holland Gordon and Breach, Science Publishers, New York, 1965.

13. Apollo/Soyuz Test Project — Joint USA/USSR Project Technical Proposal ASTP 10000, July 17, 1972.

14. Smart, W. S.: Celestial Mechanics. John Wiley and Sons, Inc., New York, 1953.

APPROVAL

SPACE SHUTTLE RENDEZVOUS, RADIATION, REENTRY ANALYSIS

By Dave M. McGlathery

The information in this report has been reviewed for security classification. Review of any information concerning Department of Defense or Atomic Energy Commission programs has been made by the MSFC Security Classification Officer. This report in its entirety, has been determined to be unclassified.

This document has also been reviewed and approved for technical accuracy.

E. D. GEISSLER
Director, Aero-Astrodynamics Laboratory